SKB

TECHNICAL REPORT 94-16

Kinetic and thermodynamic studies of uranium minerals

Assessment of the long-term evolution of spent nuclear fuel

Ignasi Casas[1], Jordi Bruno[1], Esther Cera[1],
Robert J Finch[2], Rodney C Ewing[2]

1 MBT Tecnología Ambiental, Cerdanyola, Spain
2 Department of Earth and Planetary Sciences, University of New Mexico, Albuquerque, NM, USA

October 1994

SVENSK KÄRNBRÄNSLEHANTERING AB
SWEDISH NUCLEAR FUEL AND WASTE MANAGEMENT CO

BOX 5864 S-102 40 STOCKHOLM
TEL. 08-665 28 00 TELEX 13108 SKB
TELEFAX 08-661 57 19

KINETIC AND THERMODYNAMIC STUDIES OF URANIUM MINERALS

ASSESSMENT OF THE LONG-TERM EVOLUTION OF SPENT NUCLEAR FUEL

Ignasi Casas[1], Jordi Bruno[1], Esther Cera[1], Robert J Finch[2], Rodney C Ewing[2]

1 **MBT Tecnología Ambiental, Cerdanyola, Spain**
2 **Department of Earth and Planetary Sciences, University of New Mexico, Albuquerque, NM, USA**

October 1994

ABSTRACT (English)

We have studied the dissolution behavior of uraninite, becquerelite, schoepite and uranophane. The information obtained under a variety of experimental conditions has been combined with extensive solid phase characterizations, performed on both leached and unleached samples. The overall objective is to construct a thermodynamic and kinetic model for the long-term oxidation alteration of UO_2(s), as an analogy of the spent nuclear fuel matrix.

We have determined the solubility product for becquerelite ($\log K_{s0} = 32.7 \pm 1.3$) and uranophane ($\log K_{s0} = 7.8 \pm 0.8$). In some experiments, the reaction progress has shown initial dissolution of uranophane followed by precipitation of a secondary solid phase, characterized as soddyite. The solubility product for this phase has been determined ($\log K_{s0} = 3.0 \pm 2.9$).

We have studied the kinetics of dissolution of uraninite, uranophane and schoepite under oxidizing conditions in synthetic granitic groundwater. BET measurements have been performed for uraninite and uranophane. For schoepite, the measurement has not been performed due to the lack of sufficient amount of sample. The normalized rates of dissolution of uraninite and uranophane have been calculated, referred to the uranium release, as $1.97 \cdot 10^{-8}$ moles h^{-1} m^{-2} and $4.0 \cdot 10^{-9}$ moles h^{-1} m^{-2}, respectively. For schoepite, the dissolution process has shown two different rates, with a relatively fast initial dissolution rate of $1.97 \cdot 10^{-8}$ moles h^{-1} followed, after approximately 1000 hours, by a slower one of $1.4 \cdot 10^{-9}$ moles h^{-1}. No formation of secondary phases has been observed in those experiments, although final uranium concentrations have in all cases exceeded the solubility of uranophane, the thermodynamically more stable phase under the experimental conditions.

ABSTRACT (Swedish)

Vi har studerat upplösningen av uraninit, becquerelit, schoepit och uranofan. Den information som erhållits under olika experimentförhållanden har kombinerats med omfattande fast fas karakteriseringar som utförts på såväl lakade som olakade prov. Målet med arbetet är att bygga en termodynamisk och kinetisk modell för den långsiktiga oxidationsförändringen av UO_2(s) som en analogi till använt bränsle.

Vi har bestämt löslighetsprodukten för becquerelit ($\log K_{s0} = 32.7 \pm 1.3$) och uranofan ($\log K_{s0} = 7.8 \pm 0.8$). I några av experimenten har reaktionsförloppet visat initial upplösning av uranofan följt av utfällning av en sekundär

fas, karakteriserad som soddyit. Löslighetsprodukten för denna fas har bestämts ($\log K_{s0} = 3.0 \pm 2.9$).

Vi har studerat upplösningskinetiken för uraninit, uranofan och schoepit under oxiderande förhållanden i syntetiskt grundvatten. BET mätningar har gjorts för uraninit och uranofan. För schoepit har mätningen inte kunnat göras på grund av otillräcklig provmängd. De normaliserade upplösningshastigheterna har för uraninit och uranofan beräknats till $1.97 \cdot 10^{-8}$ mol h^{-1} m^{-2} respektive $4.0 \cdot 10^{-9}$ mol h^{-1} m^{-2} avseende uranfrigörelsen. För schoepit har upplösningsprocessen visat två olika hastigheter med en relativt snabb initial upplösning på $1.97 \cdot 10^{-8}$ mol h^{-1} följd efter ca 1000 timmar av en långsammare på $1.4 \cdot 10^{-9}$ mol h^{-1}. Ingen bildning av sekundära faser har observerats i dessa experiment fastän urankoncentrationerna i samtliga fall överskred lösligheten för uranofan, som är termodynamiskt mer stabil under experimentförhållandena.

KINETIC AND THERMODYNAMIC STUDIES OF URANIUM MINERALS

ASSESSMENT OF THE LONG-TERM EVOLUTION OF SPENT NUCLEAR FUEL

Ignasi Casas, Jordi Bruno, Esther Cera
MBT Tecnología Ambiental, Cerdanyola, Spain

Robert J Finch, Rodney C Ewing
Department of Earth and Planetary Sciences,
University of New Mexico, Albuquerque, NM, USA

October 1994

Keywords: Solubility, Uranium natural analogues, Uraninite, Becquerelite schoepite, Uranophane

TABLE OF CONTENTS

GLOSSARY

Glossary of mineral names that we will refer throughout the report, together with their respective ideal chemical formula.

Mineral	Formula
alunite	$KAl_3(SO_4)_2(OH)_6$
asbolane	$(Co,Ni)_{1-y}(Mn^{+4}O_2)_{2-x}(OH)_{2-2y+2x} \cdot nH_2O$
becquerelite	$Ca[(UO_2)_6O_4(OH)_6] \cdot 8H_2O$
billietite	$Ba[(UO_2)_6O_4(OH)_6] \cdot 8H_2O$
calcite	$CaCO_3$
cattierite / vaesite	CoS_2 / NiS_2
chlorite	$(Fe^{+2},Mg)_5Al(Si_3Al)O_{10}(OH)_8$
coffinite	$USiO_4 \cdot nH_2O$
galena	PbS
illite	$(K,H_3O)(Al,Fe,Mg)_2(Si,Al)_4O_{10}[(OH)_2,H_2O]$
kasolite	$PbUSiO_6 \cdot H_2O$
plumbojarosite	$PbFe_6^{+3}(SO_4)_4(OH)_{12}$
quartz	SiO_2
schoepite-I	$UO_3 \cdot (2+x)H_2O$
schoepite-II	$UO_3 \cdot 2H_2O$
dehydrated schoepite	$UO_3 \cdot 0.8H_2O$ - $UO_3 \cdot H_2O$
sklodowskite	$(Mg,Ni)[(UO_2)(SiO_3OH)]_2 \cdot 5H_2O$
soddyite	$(UO_2)_2(SiO_4) \cdot 2H_2O$
uraninite	$(U^{+4},U^{+6},Pb,Ca,Y,REE)O_{2+x}$
α-uranophane	$Ca[(UO_2)(SiO_3OH)]_2 \cdot 5H_2O$
β-uranophane	$Ca[(UO_2)(SiO_3OH)]_2 \cdot 5H_2O$

INTRODUCTION

The performance assessment of HLNW repositories requires the long-term description of the behavior of the waste matrix. This is basically done by using the experience from leaching experiments of actual spent fuel to derive kinetic and thermodynamic models for the dissolution of spent fuel under repository conditions.

However, the time scales of spent nuclear fuel dissolution studies is of the order of 2 to 10 years, while the performance of a spent fuel repository should be assessed for much longer times (10^5-10^6 years). These time scales can be bridged using appropriate natural phases that give insight into the critical steps for the oxidative alteration of spent fuel in granitic environments.

Studies of uranium deposits have combined the measured groundwater compositions with the identification of the minerals in contact with the solution. Understanding the geochemical and hydrologic conditions and result of the formation and alteration of uranium minerals is important in understanding the behavior of uranium in groundwaters associated with spent fuel repositories. Among those, the Shinkolobwe site in Zaire constitutes a good example of the extensive alteration of uraninite, while the Cigar Lake site in Canada provides an example of uranium immobilization under reducing conditions.

An schematic pathway for the oxidative alteration of UO_2(s) (similarly as the one described by Vochten, 1991 and references therein) can be depicted as follows:

1.- Initial radiolytic surface oxidation of the UO_2(s):

$$UO_2 + \tfrac{x}{2} O_2 \Leftrightarrow UO_{2+x}$$

2.- Full oxidation to U(VI)-hydr-oxides, sometimes including cations present in groundwaters (i.e., calcium, potassium,...):

$$UO_{2+x} + (\tfrac{1-x}{2})O_2 + 2H_2O \Leftrightarrow UO_3 \cdot 2H_2O$$

$$6UO_{2+x} + O_2 + Ca^{2+} + (16-6x)H_2O \Leftrightarrow Ca(UO_2)_6O_4(OH)_6 \cdot 8H_2O + (10-12x)H^+$$

3.- The final alteration to either silicates or phosphates depends on the SiO_2 / PO_4 ratio in the groundwater:

$$Ca(UO_2)_6O_4(OH)_6 \cdot 8H_2O + 6SiO_2 + 2Ca^{2+} + 7H_2O \Leftrightarrow$$
$$\Leftrightarrow 3Ca[(UO_2)(SiO_3OH)]_2 \cdot 5H_2O + 4H^+$$

Recently, R. Ewing and coworkers at the University of New Mexico (UNM) have devoted much attention to the mineralogical and crystallographic studies of the pathways of uraninite alteration and the consequences on the long-term stability of spent fuel (Finch and Ewing, 1989; Finch and Ewing, 1991; Finch and Ewing, 1992; Janeczek and Ewing, 1992). However, in order to evaluate these mineralogical data in the perspective of the performance assessment of a spent fuel repository, the thermodynamic and kinetic constraints on the critical pathways of the oxidative alteration of uraninite should be determined in laboratory experiments in order to better understand such systems. This is necessary in order to relate the alteration pathways to the geochemistry of the contacting groundwaters.

In order to better understand the natural complexity, the systematic study of the dissolution behavior of natural uranium phases is important. Difficulties associated with understanding reactions among multiple phases can be mitigated by a detailed characterization of the solid phases. Also, examination of the leached samples at the end of the experiments provides critical information on the most recent reaction products, as well as textural information indicative of dissolution and/or precipitation.

A collaboration between MBT Tecnología Ambiental (Spain) and the Department of Earth and Planetary Sciences of the University of New Mexico (USA) is underway to better define the behavior of a series of uranium minerals that may be representative of the alteration process described. This work combines data obtained from a series of dissolution experiments under different redox conditions with a detailed characterization of the leached and unleached solid samples. However, it must be taken into account the fact that microscopic observations in an small distance scale region of the solid will be compared with a more, so to say, overall behavior of a macroscopic sample in the leaching experiments.

OBJECTIVES

The aims of this project are to establish the dissolution properties of selected natural phases of the alteration sequence:

uraninite → schoepite → uranophane

as well as related uranium phases (i.e. becquerelite).

In cooperation with R. Ewing and coworkers of the University of New Mexico (UNM), samples were selected from the following localities: Cigar Lake (Canada), Jachymov (Czech Republic), Oklo (Gabon), Shinkolowbe (Zaire), Shaba (Zaire) and Nisto Mines (Canada).

The thermodynamics and kinetics of the dissolution of these phases were experimentally determined. Leached and unleached solid phases were extensively examined at the University of New Mexico.

The data collected are used to construct a thermodynamic and kinetic model for the long-term oxidative alteration of UO_2(s).

EXPERIMENTAL

Materials

The samples were acquired from several museums and laboratories. For brevity, and in order to avoid confusion between similar samples, we will use throughout this report the UNM reference number. The list of mineral samples studied, together with their respective reference number are given in the following table.

UNM Reference No. (museum ref. no.)	**Sample Description** (predominant mineral)	**Institution**
430 (86537)	uraninite (Jachymov)	Harvard Museum
446 (105727)	uranophane (Shinkolobwe)	Harvard Museum
484 (87090)	schoepite (Shaba)	Harvard Museum
490 (10902)	becquerelite (Shinkolobwe)	Harvard Museum
514 (13291)	uranophane (Nisto Mines)	Denver Museum of Natural History
548 (91.74)	uranophane (Shinkolobwe)	Colorado School of Mines
650 (CS615-B2)	uraninite (Cigar Lake)	AECL
655 (13755)	uranophane (Shinkolobwe)	Musée Royale de l'Afrique Centrale Belgique
690 (ORZ-9-005)	uraninite (Oklo)	Los Alamos N.L.

Localities were selected based on the fact that the Shinkolobwe site is an example of extreme alteration of uraninite under oxidizing conditions, while the Cigar Lake deposit may be an example of long-term preservation of the uraninite under reducing conditions. The Oklo site is important because it is a natural reactor presently studied as a natural analogue site.

Minerals were separated by hand from other mineral inclusions before starting the experiments, but it is important to note that the macroscopic appearance of the solid phase does not assure chemical purity due to the

inability to separate microscopic inclusions. The chemical composition of each solid phase was determined as part of the detailed sample characterization completed at UNM.

Experiments were conducted using two different leachants. Under anoxic conditions, double distilled water was used, while all the other experiments were performed using a synthetic granitic groundwater, the composition of which is given in the following table.

Element	Concent. (mM)
Li	4.43
Na	1.47
K	0.17
Mg	0.13
Ca	0.04
Al	$< 5x10^{-3}$
silicates	1.14
phosphates	0.03
sulfates	0.02
nitrates	5.00
bicarbonates	4.015
fluoride	0.04
chloride	0.075

Solid phase characterization

In this and subsequent sections dealing with the characterization of the solid samples, we will present a summary of the main features that were observed during an extensive examination of the leached and unleached solid phases.

Several methods were used for the characterization of both leached and unleached solid phases. For the unleached samples, the analytical methods used were optical microscopy, XRD, EMPA (EDS,WDS), and conventional SEM (also Environmental SEM) with EDS. For the leached samples, both conventional SEM and Environmental SEM, along with EDS, were used. A brief description of these techniques is presented below.

X-RAY DIFFRACTION (XRD) powder data provides for the determination of unit cell parameters and for relatively rapid phase identification; it is especially useful for identifying several phases simultaneously and their relative proportions from multi-phase samples. The insensitivity of XRD to phases which are present in amounts less than approximately ten volume percent makes the identification of minor phases difficult. XRD is also relatively insensitive to amorphous material.

OPTICAL MICROSCOPY was employed for preliminary phase identification, reconnaissance of textural relationships and for determining phase relationships, where appropriate. The relative abundance of phases present may also be estimated.

SCANNING ELECTRON MICROSCOPY (SEM) allows phase identification (when combined with energy dispersive x-ray spectroscopic analysis, EDS) and examination of phase relationships and textural features. Two types of SEM were employed for studying bulk samples: 1) a conventional high vacuum (ca. 10^{-5} torr) and 2) a high pressure (2- 10 torr). Samples studied using the ESEM did not require any special handling, and, for the leached samples, specimens were mounted in the ESEM directly from solution.

Polished thin sections were also analyzed with SEM using back-scattered electron imaging (BSEI). This technique is sensitive to differences in average atomic number (due to composition or density). Phase relationships among uranium phases, often indistinguishable using optical methods, are readily distinguished using BSEI.

ELECTRON MICROPROBE ANALYSIS (EMPA) provides quantitative chemical analysis of microscopically small grains (to 1 μm). Analyses may include chemical information from adjacent material. Polished thin sections were analyzed using an automated microprobe with five spectrometers and quantitative EDS.

Experimental procedure

The experiments were performed under three different redox conditions: reducing, anoxic and oxidizing.

All the batch studies were performed at room temperature. An orbital stirrer was used to keep the solution homogeneously mixed and to minimize physical damage of the solid phase.

Mineral samples used ranged from 0.02 g. to 1 g.

Reducing conditions

These experiments were carried out in a glass vessel, with a mixture of H_2/1% CO_2 atmosphere, in the presence of a palladium catalyst and using synthetic granitic groundwater as the leachant. The initial volume of the test solution was 450 ml.

The minerals included in this series of experiments were:

- *uraninite* (650) from Cigar Lake (1.0061 g).

- *uraninite* (430) from Jachymov (0.7118 g).

- *uraninite* (690) from Oklo (1.0678 g).

The intention of this series of experiments was to collect equilibrium data to perform a thermodynamic study on the selected samples.

The three samples that were selected, one from each specimen, did not show macroscopic inclusions, and they were used directly as provided. The solid phases were previously treated for 1-2 days with a diluted perchloric acid solution (≅10%) under reducing conditions. In this way we expected to eliminate fine particles and/or secondary solid phases. They were subsequently washed several times with the final leachant solution to eliminate the acid solution left on the solid surface.

Anoxic conditions

These experiments used a N_2 atmosphere, using double distilled water as leachant.

The minerals studied in this series of experiments were:

- *uranophane* (446) from Shinkolobwe (0.2468 g), in a glass vessel with an initial volume of solution of 400 ml.

- *uranophane* (655) from Shinkolobwe (0.0553 g), in a polyethylene bottle (initial volume: 450 ml).

- *uranophane* (514) from Nisto Mines (0.0841 g), in a polyethylene bottle (initial volume of solution: 1000 ml).

- *becquerelite* (490) from Shinkolobwe (0.0215 g), in a polyethylene bottle (450 ml).

The dissolution of these samples was followed as a function of time. In case equilibrium was reached, the pH of the test solution was changed and the sequence restarted. The attainment of equilibrium was assumed when both aqueous uranium concentration and pH readings remained constant for several days.

The use of polyethylene bottles in three of the experiments was due to our intention to follow the Si and Ca release for the uranophane, as well as the Ca release for the becquerelite sample, in addition to the U dissolution.

In the first case, uranophane (446) was not separated from other mineral inclusions, and the solid sample was used as received. In the other cases, crystals of uranophane (665, 514) and becquerelite (490), respectively, were separated by hand and macroscopic inclusions eliminated.

Minerals were initially washed with double distilled water in a N_2 atmosphere for 3-4 hours, followed by the replacement of this solution by the fresh double distilled water to be used as final leachant.

Oxidizing conditions

These experiments were performed in contact with air, in a polyethylene bottle, using the synthetic granitic groundwater as leachant (initial volume of 450 ml).

The minerals studied in this series were:

- *uraninite* (650) from Cigar Lake (0.5580 g).

- *schoepite* (484) from Shaba (0.1225 g).

- *uranophane* (548) from Shinkolobwe (0.0353 g).

The dissolution of uranium from these samples was followed as a function of time.

Schoepite and uranophane were separated by hand from other macroscopic mineral inclusions. Uraninite was used as provided, as no macroscopic inclusions were observed. Minerals were initially washed for 1-2 hours with

double distilled water before experiments were started with the synthetic granitic groundwater.

Independently of the redox conditions, pH values were periodically monitored by means of a previously calibrated combined glass electrode.

Under reducing conditions, we also followed the redox potential using a platinum electrode and the reference of the combined glass electrode. The Eh was then calculated using 222 mV as the potential at 25°C of the Ag/AgCl reference electrode.

Changes of pH, when necessary, were made using either sodium hydroxide or perchloric acid.

Experiments under reducing and anoxic conditions used an oxygen trap composed of an acidic solution of chromium chloride with a Zn/Hg amalgam to prevent the introduction of oxygen gas into the reactor (figure 1).

As a guide to the reader to more easily follow the subsequent sections, the different experiments are summarized in the following table.

Redox conditions	Leaching solution	Solid sample	Vessel
reducing	synthetic groundwater	uraninite sample #650	glass
reducing	synthetic groundwater	uraninite sample #430	glass
reducing	synthetic groundwater	uraninite sample #690	glass
anoxic	double distilled water	uranophane sample #446	glass
anoxic	double distilled water	uranophane sample #655	polyethylene
anoxic	double distilled water	uranophane sample #514	polyethylene
anoxic	double distilled water	becquerelite sample #490	polyethylene
oxidizing	synthetic groundwater	uraninite sample #650	glass
oxidizing	synthetic groundwater	schoepite sample #484	glass
oxidizing	synthetic groundwater	uranophane sample #548	glass

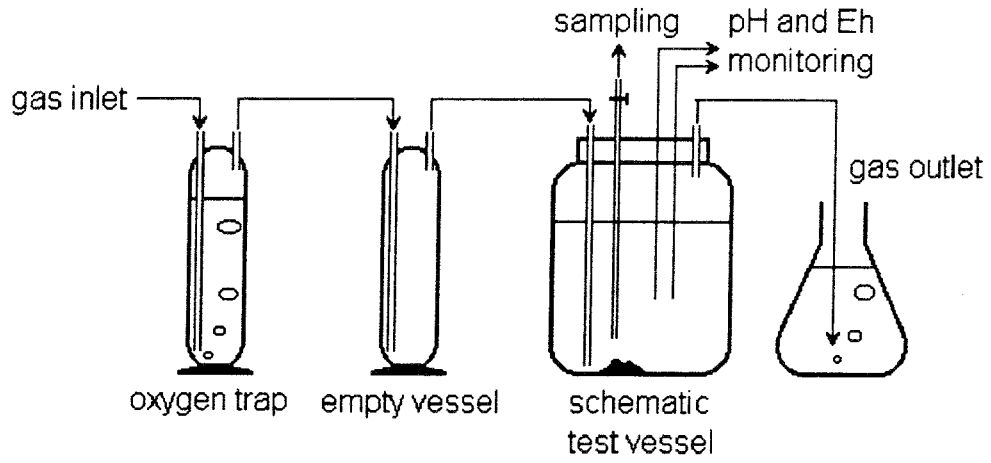

Figure 1.- Schematic view of the experimental system used under reducing and anoxic conditions.

Analytical methods

Uranium concentrations in solution were measured, for all the experiments, for each sample taken. Silicon and calcium were also determined at selected samples in the three experiments performed under anoxic conditions in polyethylene bottles.

For each sample three aliquots of 2 ml were taken for uranium determinations, and two aliquots of 10 ml were used for silicon and calcium determinations. Samples were immediately filtered through MILLIPORE membranes of 0.22 μm nominal pore size, to remove possible solid particles. When it was necessary to store the solutions for some time before analyses, they were acidified with a small volume of concentrated HNO_3.

Uranium was analyzed with a Scintrex UA-3 laser fluorescence analyzer. The basis of this technique is the increase in fluorescence due to the uranium content when a commercial buffer phosphate (FLURAN) is added to the solution. The values obtained are compared with a uranyl nitrate standard solution. Using the standard addition method, the detection limit is 0.01 ng dm^{-3} with an estimated associated error of ± 30% (Robbins 1978a, 1978b). For uranium levels of the order of 1 ppb, the associated error is estimated to be less than 10%.

Iron can interfere with this analytical method, because it acts as a "quencher" of the fluorescence signal. Since some of the minerals have associated iron bearing inclusions, we had to ensure that our uranium determinations were free of interferences. We checked this point in all the experiments and the

error associated to the iron content was found to be negligible in all cases, according to literature (de Pablo et al., 1992).

Silicon and calcium were analyzed by means of an Inductively Coupled Plasma Spectrometer (ICP) with ultrasound nebulizer.

RESULTS AND DISCUSSION

In order to avoid confusion, we present the results obtained from the sample characterization of the unleached and leached samples in a single section, and the results from the leaching experiments in a subsequent section. The final discussion integrates the results of the solid phase characterization with the results of the solution analyses.

Solid samples description

Unleached samples

Uraninite from Jachymov, Czech Republic (#430)

Was a massive, fine-grained uraninite with numerous calcite veins cross-cutting the uraninite. At least, two different types of uraninites were evident identified by the change in the image contrast under BSEI, possibly due to unit cell volume differences, as well as possible compositional differences (Figure 2). The core of the grains commonly display the highest contrast, both optically and with BSEI. The unit cell parameter for the synthetic cubic uranium oxides decrease with increased oxidation state up to approximately $UO_{2.25}$(s), and for a given chemical composition, this is probably true for natural uraninites as well. The brightest region probably corresponds to the smallest unit cell volume. No differences in chemistry were detected between the different regions. Transmission electron microscopy (TEM) showed that the grain size of the uraninites were exceptionally small (<10 nm).Coffinite has been reported from Jachymov (Janeczek, 1991); however, coffinite is not evident from the XRD powder data.

Minerals identified - bulk sample

Mineral	Ideal Formula	Vol.% (est.)
uraninite	$(U^{+4},U^{+6},Pb,Ca,Y,REE)O_{2+x}$	85 - 90
calcite	$CaCO_3$	10 - 15
coffinite (?)	$USiO_4 \cdot nH_2O$	?

Uraninite from Cigar Lake, Canada (#650)

Was massive and compact in hand sample. A large portion contained uraninite grains with an extremely fine-grained proportion (~10 nm particle sizes) that occurs at the interface between the coarse-grained uraninite and the clay matrix. The solid was composed of approximately fifty volume percent clay

matrix that contained mainly illite and chlorite with variable-sized uraninite grains (Figure 3).

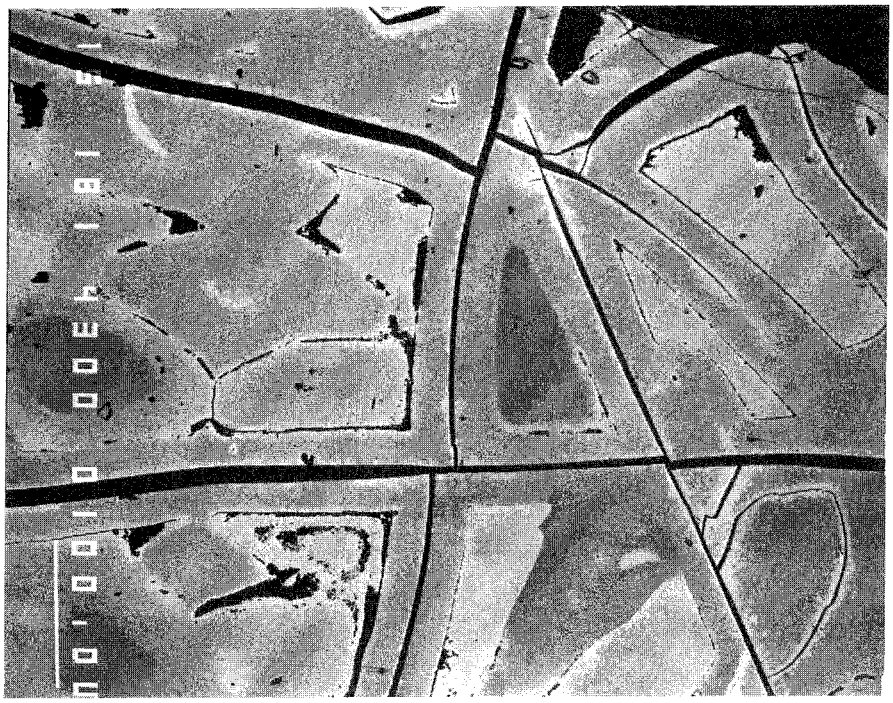

FIGURE 2. BSE image of polished section of Jachymov uraninite pre-leach, veined by calcite (darkest contrast). BSE reflectance shows three regions, suggesting different densities. The brightest regions correspond to the highest density material.

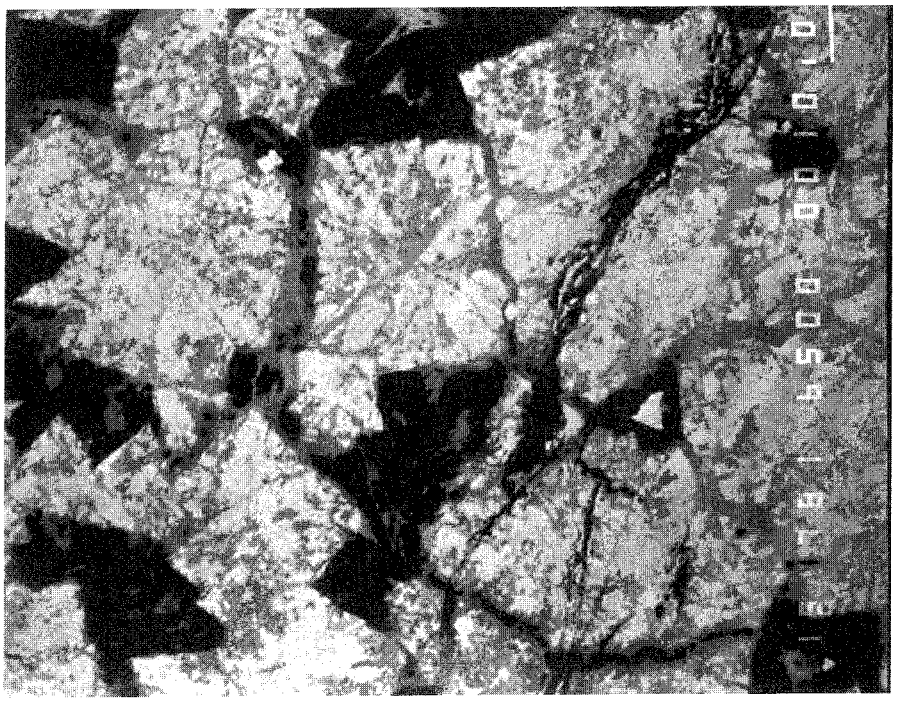

FIGURE 3. BSE image of polished section of unleached Cigar Lake uraninite (bright) in an illite matrix (dark), partially replaced by chlorite (light gray).

The solid was cross-cut by several narrow (0.1-1.0 mm wide) veins of mixed Al-rich illite and Fe-rich chlorite. Small inclusions of a Mg-silicate, probably antigorite, also occur within these veins.

Janeczek and Ewing (1992), in their detailed description of uraninite samples from this location, distinguished two uraninites in this solid phase, a Pb-rich uraninite, with 10-11 weight percent PbO, and a Pb-poor uraninite with less than ten weight percent PbO. Although no coffinite was identified, Janeczek and Ewing (1992) identified coffinite in other Cigar Lake samples from the same drill core (#220).

Minerals identified - bulk sample

Mineral	Ideal Formula	Vol.% (est.)
uraninite	$(U^{+4},U^{+6},Pb,Ca,Y,REE)O_{2+x}$	45 - 55
"illite" (Al-rich)	$(K,H_3O)(Al,Fe,Mg)_2(Si,Al)_4O_{10}[(OH)_2,H_2O]$	30-35
"chlorite" (Fe-rich)	$(Fe^{+2},Mg)_5Al(Si_3Al)O_{10}(OH)_8$	20
antigorite (?)	$Mg_3Si_2O_5(OH)_4$	< 5
galena	PbS	< 5
chalcopyrite	$CuFeS_2$	< 5
coffinite (?)	$USiO_2 \cdot nH_2O$	?
pyrite (?)	FeS_2	?

Uraninite from Oklo, Gabon (#690)

Was massive, composed of fractured and broken grains of uraninite within a matrix of uraninite and opaque organic material (Figure 4). Chlorite, illite and minor calcite fill fractures and voids within both the uraninite and the organic matrix. Base metal sulfides occur within the clay-filled veins and are commonly associated with uraninite grains.

The grain sizes of the uraninite crystals vary widely from approximately 0.5 mm to less than 100 μm. Coffinite has not been identified in this sample, but reactor zone nine, from which this solid was obtained, contains abundant coffinite (Janeczek and Ewing, 1992).

Minerals identified - hand separated

Mineral	Ideal Formula	Vol.% (est.)
uraninite	$(U^{+4},U^{+6},Pb,Ca,Y,REE)O_{2+x}$	90 - 95
galena	PbS	< 5
illite	$(K,H_3O)(Al,Fe,Mg)_2(Si,Al)_4O_{10}[(OH)_2,H_2O]$	< 5
chlorite	$(Fe^{+2},Mg)_5Al(Si_3Al)O_{10}(OH)_8$	< 5
kaolinite (?)	$Al_2Si_2O_5(OH)_4$	< 5
organic material	complex hydrocarbons with S, P	< 5
quartz	SiO_2	< 5
coffinite (?)	$USiO_4 \cdot nH_2O$	?

FIGURE 4. Photomicrograph of unleached Oklo uraninite (bright), showing fractured and embayed uraninite grains within darker organic material. 2.0 mm across

Uranophane from Shinkolobwe, Zaire (#446)

Contained crystals of α-uranophane as the only uranium phase positively identified, radiating from a central core of embayed quartz grains, a mixture of plumbojarosite and alunite, and an undetermined black phase that may be asbolane (Co-Ni-Mn phase) (Figure 5).

XRD powder data for the bulk sample indicated that uranophane predominated (ca. 80-85 vol.%), and quartz was also present (5-10 vol.%). The uranophane was nearly ideal, chemically, although dehydrated and slightly deficient in Si. The formula calculated from the chemical data is:

$$Ca_{0.94}U_{2.10}Si_{1.88}O_{11} \cdot 3.7H_2O$$

This sample was leached without previous hand separation of non-uranium phases.

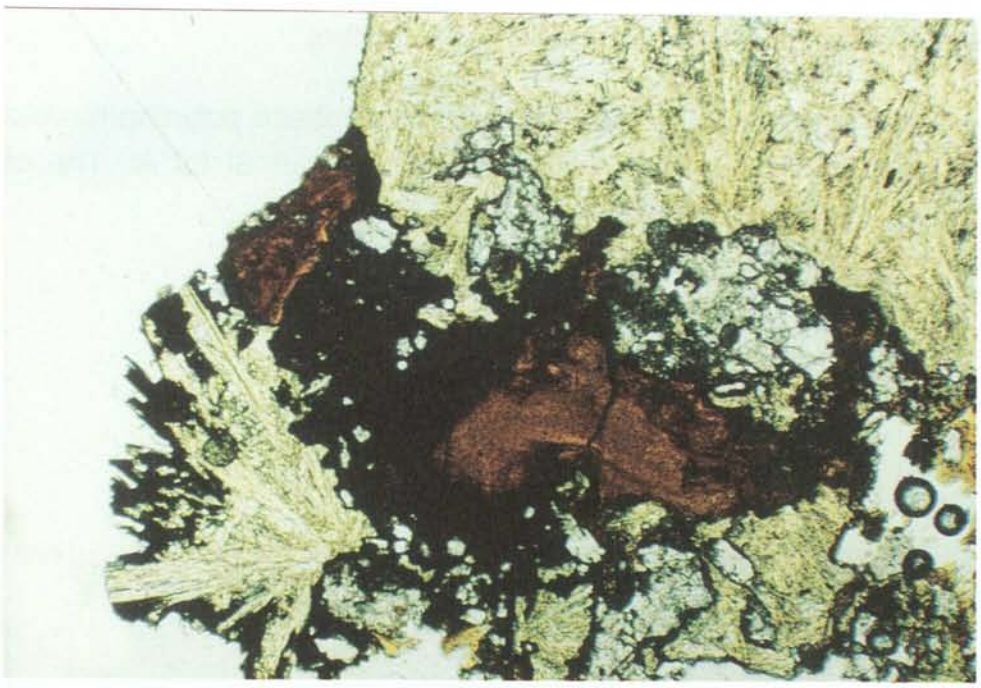

FIGURE 5. Photomicrograph of a polished section of unleached uranophane from Shinkolobwe (446). Reddish brown plumbojarosite-alunite and black asbolane occupy the core. Quartz is also abundant. 2.8 mm across

Minerals identified - bulk sample

Mineral	Ideal Formula	Vol. %
α-uranophane	$Ca[(UO_2)(SiO_3OH)]_2 \cdot 5H_2O$	80 - 85
quartz	SiO_2	5
chlorite	$(Fe^{+2},Mg)_5Al(Si_3Al)O_{10}(OH)_8$	< 5
plumbojarosite	$PbFe_6^{+3}(SO_4)_4(OH)_{12}$	< 5
alunite	$KAl_3(SO_4)_2(OH)_6$	< 5
goethite (?)	$Fe^{+3}O(OH)$	< 5
asbolane (?)	$(Co,Ni)_{1-y}(Mn^{+4}O_2)_{2-x}(OH)_{2-2y+2x} \cdot nH_2O$	5
kasolite (?)	$PbUSiO_6 \cdot H_2O$	< 1

Uranophane from Nisto Mines, Canada (#514)

Contained two polymorphs of α- and β-uranophane. The uranophane also contained abundant quartz (approx. 50 volume percent). Uranophane filled fractures and grain boundaries between the quartz grains, and it appeared to have replaced the quartz, the grains of which were embayed (Figure 6). The two polymorphs are distinguished by differences in their space groups and unit cell parameters. The only significant difference observed between the two polymorphs was that the uranophanes occurred in two predominant grain sizes. These were not separated by a sharp boundary, but by a continuous change in grain size over 100 to 200 microns. Much of the uranophane on the surface, however, occurs as small (1 μm) clusters

The average chemical analysis for both uranophane polymorphs was nearly ideal, with some substitution of Ca by Pb and of Si by Al. The chemical formula calculated on the basis of eleven oxygens is:

$$(Ca_{0.80}Pb_{0.015})(Si_{1.88}Al_{0.03})U_{2.11}O_{11} \cdot 4.2H_2O$$

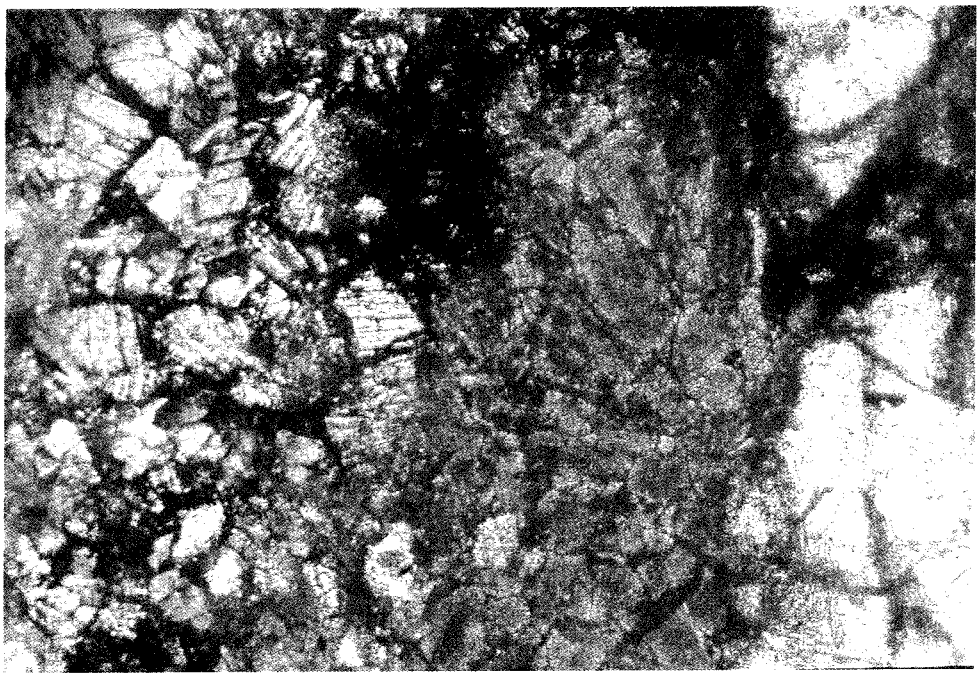

FIGURE 6. Photomicrograph of unleached uranophane vein from Nisto Mines (514), showing uranophane grain size variation. Yellow and white uranophane (center and left) and white quartz (right). Dark material is Fe-oxide and monazite. 2.0 mm across

Minerals identified - bulk sample

Mineral	Ideal Formula	Vol.% (est.)
quartz	SiO_2	50
α-uranophane	$Ca[(UO_2)(SiO_3OH)]_2 \cdot 5H_2O$	30
β-uranophane	$Ca[(UO_2)(SiO_3OH)]_2 \cdot 5H_2O$	20
monazite-(Ce)	$CePO_4$	< 5
xenotime-(Y) (?)	YPO_4	< 1
unidentified Fe^{+3}-oxide	$Fe_2O_3 \cdot nH_2O$?	< 5
goethite (?)	$Fe^{+3}O(OH)$	

Uranophane from Shinkolobwe, Zaire (#655)

Contained acicular crystals of α-uranophane which radiate from a common center of uraninite. Soddyite (approximately 10 volume percent) is intergrown with the uranophane. Minor schoepite is also present (Figure 7).

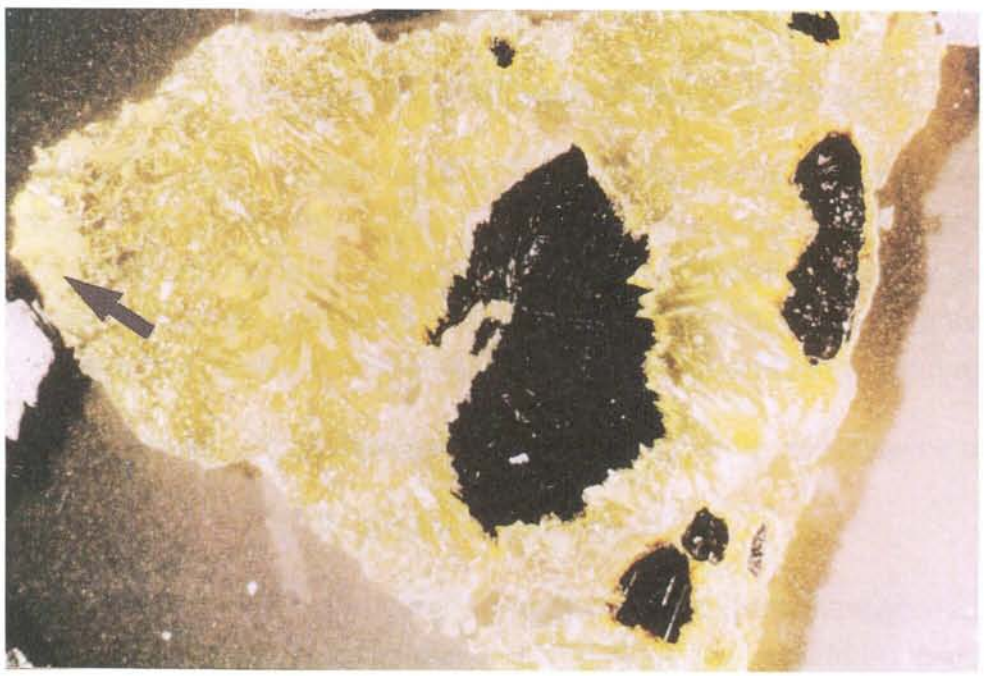

FIGURE 7. Photomicrograph of a polished section of unleached uranophane from Shinkolobwe (655), showing the central core of black uraninite, which is rimmed by a thin

layer of uranyl oxide hydrates. The arrow at left indicates a large inclusion of soddyite. 1.5 cm across

The soddyite crystals (50-200 μm) are intergrown with the uranophane in cavities. Many small soddyite crystals were euhedral and uncorroded, but most of the soddyite was fine-grained and massive, filling gaps between the uranophane needles. This texture indicates that soddyite formation postdates the formation of the uranophane.

The composition of the uranophane, was also remarkably ideal:

$$Ca_{0.89}U_{2.12}Si_{1.88}O_{11} \cdot 4.4H_2O$$

Minerals identified - hand separated

Mineral	Ideal Formula	Vol.% (est.)
α-uranophane	$Ca[(UO_2)(SiO_3OH)]_2 \cdot 5H_2O$	80 - 85
soddyite	$(UO_2)_2(SiO_4) \cdot 2H_2O$	10 - 15
quartz	SiO_2	5
schoepite	$UO_3 \cdot 2H_2O$	< 5
becquerelite	$Ca[(UO_2)_6O_4(OH)_6] \cdot 8H_2O$	< 1
chlorite	$(Fe^{+2},Mg)_5Al(Si_3Al)O_{10}(OH)_8$	< 1
ianthinite (?)	$UO_2 \cdot 5UO_3 \cdot 10H_2O$	?

Becquerelite from Shinkolobwe, Zaire (#490)

Crystals with well formed euhedral, tabular habits, consist of a three phase mixture of becquerelite (approximately 90%), dehydrated schoepite and an unidentified Pb-uranyl oxide hydrate. Several of the becquerelite crystals had been partially altered to uranophane. The intergrowth of becquerelite with Pb-uranyl oxide hydrate minerals is common in many natural samples (Figure 8).

The composition of the becquerelite is nearly ideal, the calculated formula is:

$$(Ca_{0.845}Pb_{0.05}Si_{0.1.})U_{5.97}O_{19} \cdot 8.5H_2O$$

These crystals were separated from a substrate consisting predominantly of altered uraninite. Additional phases identified in the bulk sample include kasolite, ianthinite and vandendriesscheite. These phases occur only within

the altered uraninite, not in close proximity to the becquerelite grains. They are not expected to occur in the hand-separated crystals of becquerelite.

FIGURE 8. BSE image of unleached polycrystalline bequerelite grains with abundant inclusions of an undetermined Pb-uranyl oxide hydrate.

Minerals identified - hand separated crystals

Mineral	Ideal Formula	Vol.% (est.)
becquerelite	$Ca[(UO_2)_6O_4(OH)_6]\cdot 8H_2O$	> 90
dehydrated schoepite	$UO_3\cdot 0.8H_2O$ - $UO_3\cdot H_2O$	5
unidentified Pb-UOH	$Pb_m[(UO_2)_xO_y(OH)_7]\cdot nH_2O$	< 5
α-uranophane	$Ca[(UO_2)(SiO_3OH)]_2\cdot 5H_2O$	< 5
kasolite	$(PbUSiO_6\cdot H_2O)$	
ianthinite	$UO_2\cdot 5UO_3\cdot 10H_2O$	
vandendriesscheite	$(Pb_2U_7O_{22}\cdot 22H_2O)$	
anglesite	$PbSO_4$	< 5

Schoepite from Shaba, Zaire (#484)

Contained schoepite with approximately ten volume percent of dehydrated schoepite and minor becquerelite. Both phases were essentially pure.

This sample contained numerous corroded grains, which probably is a result of dehydration that occurred during storage (Figure 9).

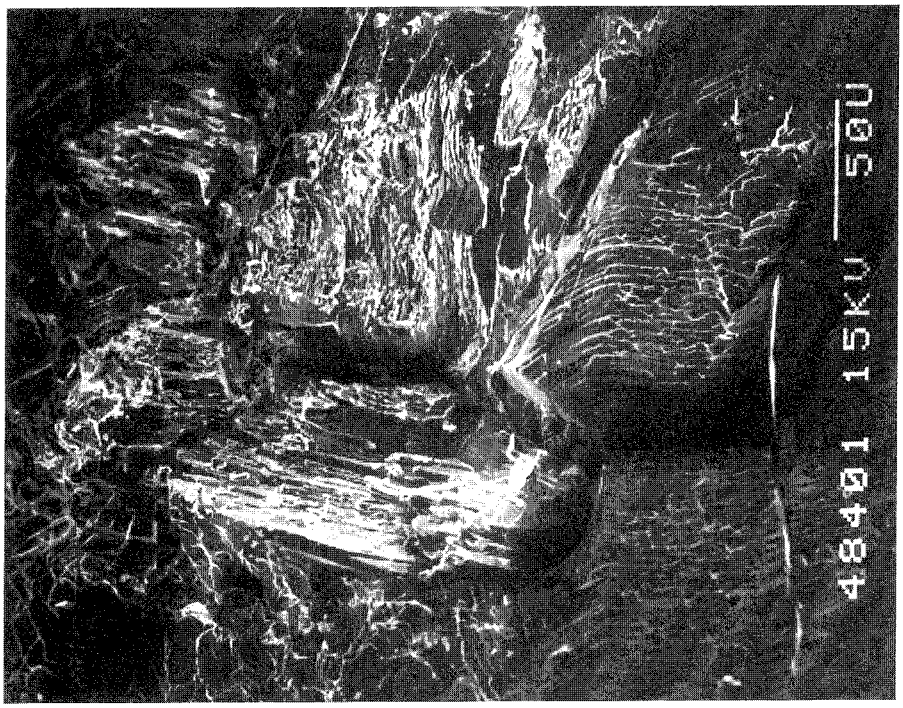

FIGURE 9. SEM image of schoepite grains in the unleached sample showing a corroded appearance.

Minerals identified - hand separated

Mineral	Ideal Formula	Vol.% (est.)
schoepite-II	$UO_3 \cdot 2H_2O$	75 - 80
dehydrated schoepite	$UO_3 \cdot 0.8H_2O$ - $UO_3 \cdot H_2O$	10 - 15
schoepite-I (?)	$UO_3 \cdot (2+x)H_2O$	< 5
becquerelite	$Ca[(UO_2)_6O_4(OH)_6] \cdot 8H_2O$	5 - 10

Uranophane from Shinkolobwe, Zaire (#548)

Was mineralogically and chemically complex. This sample contained small acicular crystals of α-uranophane and lesser amounts of Ni-sklodowskite. The sklodowskite occurred as a thin layer on the outer edge of the uranophane crust. These two phases were indistinguishable using optical methods. The uranophane contained minor Pb. The formulas calculated are:

uranophane: $(Ca_{0.89}Pb_{0.025})_{0.91}U_{2.13}Si_{1.84}O_{11} \cdot 5.33H_2O$

sklodowskite: $(Mg_{0.66}Ni_{0.15})_{0.81}U_{2.12}Si_{1.93}O_{11} \cdot 5.5H_2O$

The acicular uranophane crystals on the outer edge emanate from a dense material of massive uranophane that was in contact with a thin layer of Pb-uranyl oxide hydrates such as kasolite, schoepite and ianthinite (Figure 10).

FIGURE 10. Photomicrograph of a polished section of uranophane from Shinkolobwe (#548), illustrating the region from which the sample was derived. Black uraninite is bordered by brown kasolite and massive uranophane, Ni-sklodowskite occurs along the top of the sample. Transmitted light, plane polarized, 3.0 mm across.

Other phases present within the uranophane included soddyite, quartz and Co and Ni sulfides.

Minerals identified - hand separated

Mineral	Ideal Formula	Vol.% (est.)
α-uranophane	$Ca[(UO_2)(SiO_3OH)]_2 \cdot 5H_2O$	80 - 85
Ni-sklodowskite	$(Mg,Ni)[(UO_2)(SiO_3OH)]_2 \cdot 5H_2O$	5
meta-torbernite	$Cu[(UO_2)(PO_4)]_2 \cdot 8H_2O$	< 5
kasolite	$Pb[(UO_2)(SiO_4)] \cdot H_2O$	< 5
soddyite	$(UO_2)_2(SiO_4) \cdot 2H_2O$	< 5
quartz	SiO_2	< 5
cattierite / vaesite (?)	CoS_2 / NiS_2	< 1

Leached samples

Uraninite from Jachymov, Czech Republic (#430)

The leached solid was pitted and the vein-filling calcite has been lost, possibly explaining the disaggregation of the sample during the experiment, following the initial addition of NaOH.

FIGURE 11. SEM image of leached Jachymov uraninite displaying the differential leaching of this sample. Crystals of K-Cl phase precipitated on the sample surface following removal of the solution. Compare with figure 2.

This solid was leached differentially, regions associated with grain boundaries appeared unleached; whereas, the cores of the grains appeared to be strongly leached (Figure 11). These regions apparently correspond to the regions of low and high BSEI contrast, respectively, in the unleached sample. The leached cores displayed parallel crystallites, consistent with microstructural observations of the unleached sample using TEM.

Uraninite from Cigar Lake, Canada (#650)

From the experiment under reducing conditions. This solid decomposed to a powder after the initial addition of NaOH. The clay possibly fell off during agitation as the fine-grained uraninite disaggregated.

The mineral surface was pitted and appeared strongly corroded. Several large voids, or cavities were apparent in the larger particles (Figure 12). Most of the surface had a sponge-like texture with small pits (Figure 13) and EDS analyses revealed only U with minor Pb.

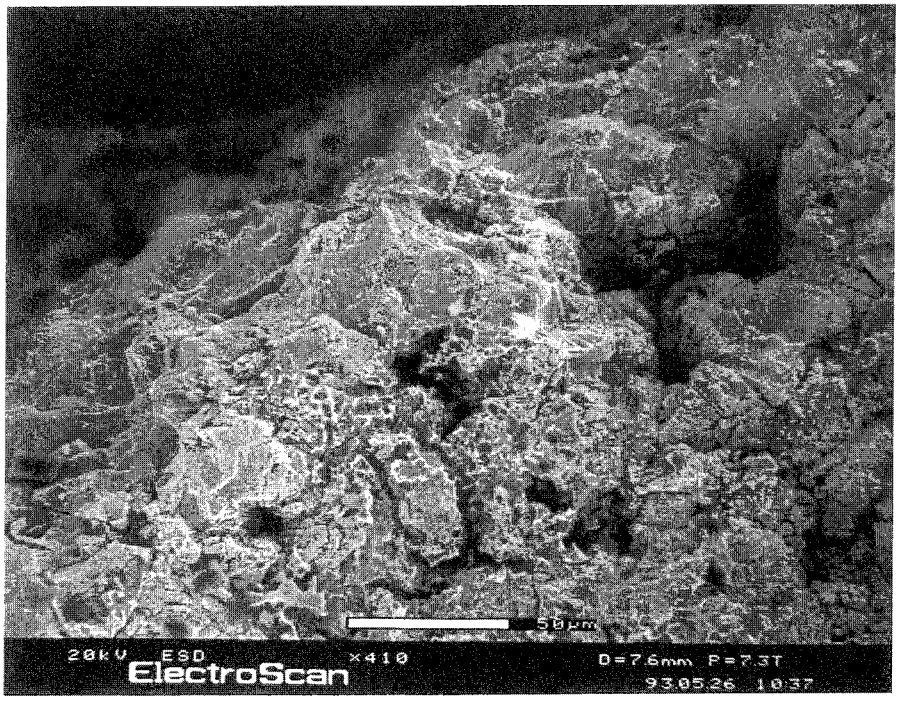

FIGURE 12. SEM image of the Cigar Lake sample leached under reducing conditions. Note the voids which presumably contained clay minerals prior to leaching.

Some unpitted surface regions were also observed. The unpitted regions commonly appeared to be covered with a smooth layer. No difference in chemical composition was detected between the pitted and unpitted regions using qualitative EDS. These regions may represent the two different uraninite compositions (low Pb and high Pb) noted for this solid (Janeczek and Ewing, 1992). The distinction between the two uraninite compositions using only EDS is difficult.

Uraninite from Oklo, Gabon (#690)

Like the other uraninite samples, after the addition of NaOH, a portion of the solid was disaggregated to a powder. Uraninite was abundant in the leached sample examined. A wide range of uraninite grain sizes and morphologies was observed. The surfaces of the uraninite grains appeared pitted and irregular. Several small tufts of a fine-grained phase were also observed, but is unidentified.

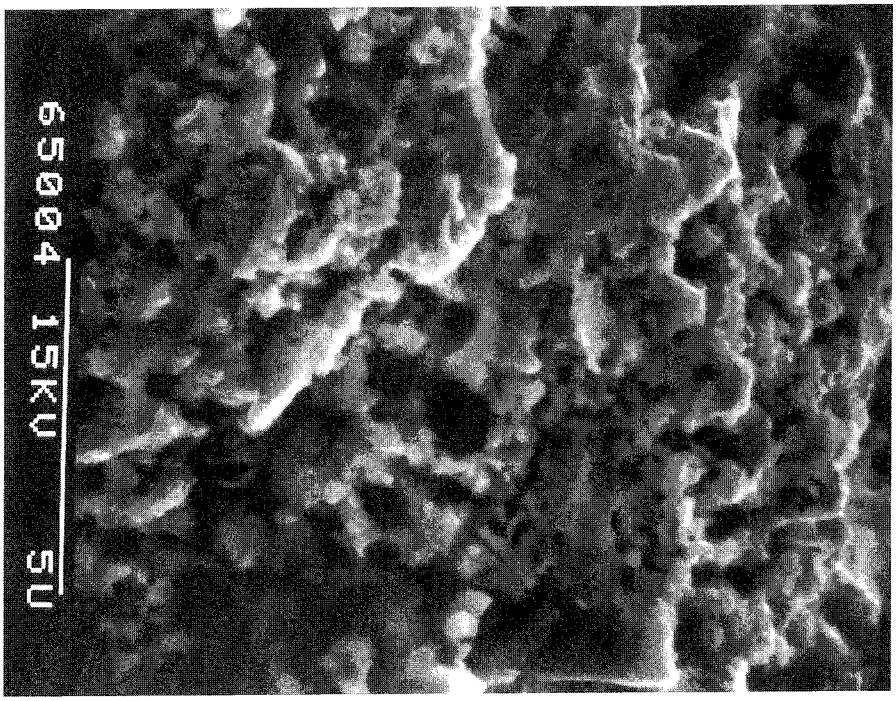

FIGURE 13. Surface of the Cigar Lake uraninite leached under reducing conditions, dried overnight. This sponge-like texture was common.

After uraninite, illite was the most common mineral identified. The illite filled numerous veins and fractures in the solid, commonly occurring as well developed, platy crystals. No sulfide minerals, identified in the unleached

specimen were detected after leaching. Organic matter, common in the unleached sample, was not positively identified.

Uranophane from Shinkolobwe, Zaire (#446)

This solid was leached without previous hand separation of non-uranium phases. The uranophane was strongly leached, with several areas displaying skeletal grains of uranophane, although several uncorroded crystals were also observed (Figure 14).

Many areas of the solid were covered by an amorphous-appearing coating, for which only U was positively detected in EDS. Several uranophane crystals were covered by spherical particles of unidentified metal oxides, similar to the unleached sample, which possibly correspond to asbolane. Mixed plumbojarosite-alunite was not detected in the leached solid.

FIGURE 14. SEM image of skeletal uranophane crystals on the surface of the sample 446 after leaching.

Uranophane from Nisto Mines, Canada (#514)

After leaching, the uranophane appeared to have been strongly corroded. Although the quartz grains were corroded, they had this same appearance in the unleached sample as well.

The sample surface had abundant well-formed soddyite crystals (5-10 μm), indicating that the transformation of uranophane to soddyite occurred via dissolution and reprecipitation during the experiment. No soddyite was detected in the unleached material (Figure 15).

Uranophane from Shinkolobwe, Zaire (#655)

All the uranophane in the leached solid was corroded, and the surface was covered by abundant small crystals (1-5 μm), probably schoepite precipitated after removal of the sample from the solution, although many precipitates appeared fibrous, resembling rutherfordine (Figure 16).

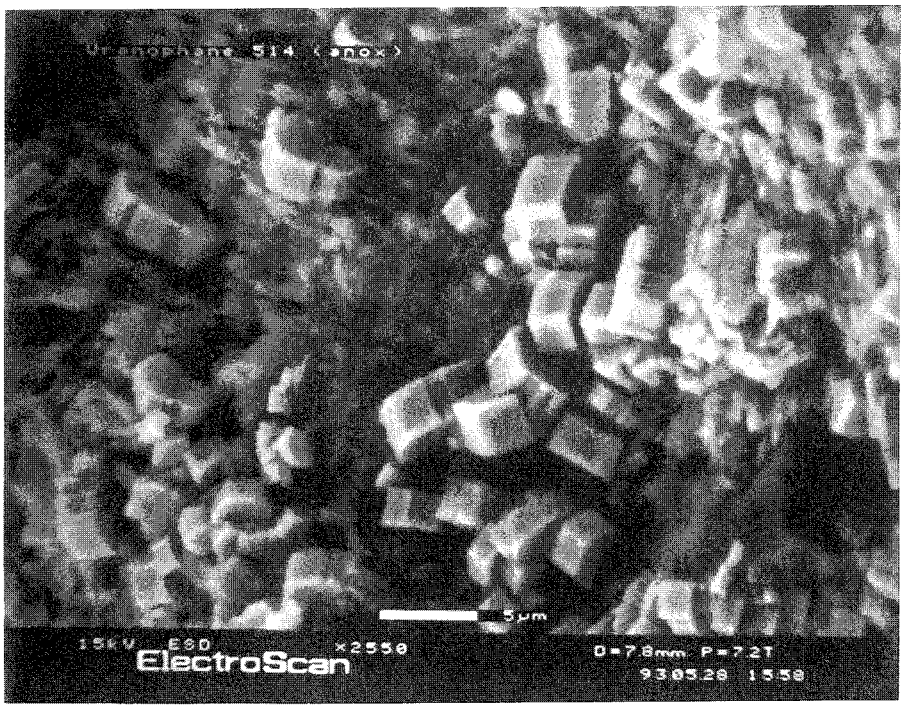

FIGURE 15. SEM image of the euhedral soddyite crystals on the surface of the sample 514 after leaching. These crystals are recently precipitated and uncorroded.

FIGURE 16. SEM image of the corroded surface of uranophane (655) after leaching. The surface is virtually covered with small crystals (EDS indicates only U, although the presence of Si cannot be ruled out), probably precipitated after removal from solution.

Schoepite also appeared to have precipitated from solution during the experiment. Two habits were evident: tabular and prismatic. The solid examined in the ESEM changed from a dark yellow when wet to a bright lemon yellow when removed from the ESEM sample chamber. This is consistent with the color change of schoepite during dehydration which probably occurred under the electron beam. Amber-brown particles removed from the solution showed only S when analyzed by EDS. The source of the S-bearing particles is unknown. One possibility is that these particles were introduced into the experiment from another source. Whether this would explain the erratic behavior of U in this experiment, or affect the experiment in other ways, is uncertain.

Becquerelite from Shinkolobwe, Zaire (#490)

The crystals examined after leaching showed virtually no evidence of pitting or corrosion. Chemical analyses by EDS indicated that all crystals were essentially becquerelite. One leached crystal contained some micron-sized inclusions of a Pb-uranyl oxide hydrate. Similar impurities were identified as inclusions within unleached becquerelite crystals.

Schoepite was not identified in the leached material, and there was not evidence for the transformation of becquerelite to schoepite. Uranophane was identified in the unleached bulk sample, but it was not apparent in the leached material. Soddyite was not identified in the unleached material, but it was present in the leached specimens. Despite the high Ca:U ratio in some of the solution aliquots, there was no strong evidence for the preferential leaching of Ca.

Uraninite from Cigar Lake, Canada (#650)

From the experiment under oxidizing conditions. In contrast with the solid leached under reducing conditions, this specimen remained intact throughout the experiment. A kinetic study was performed in this case in which the pH was not adjusted.

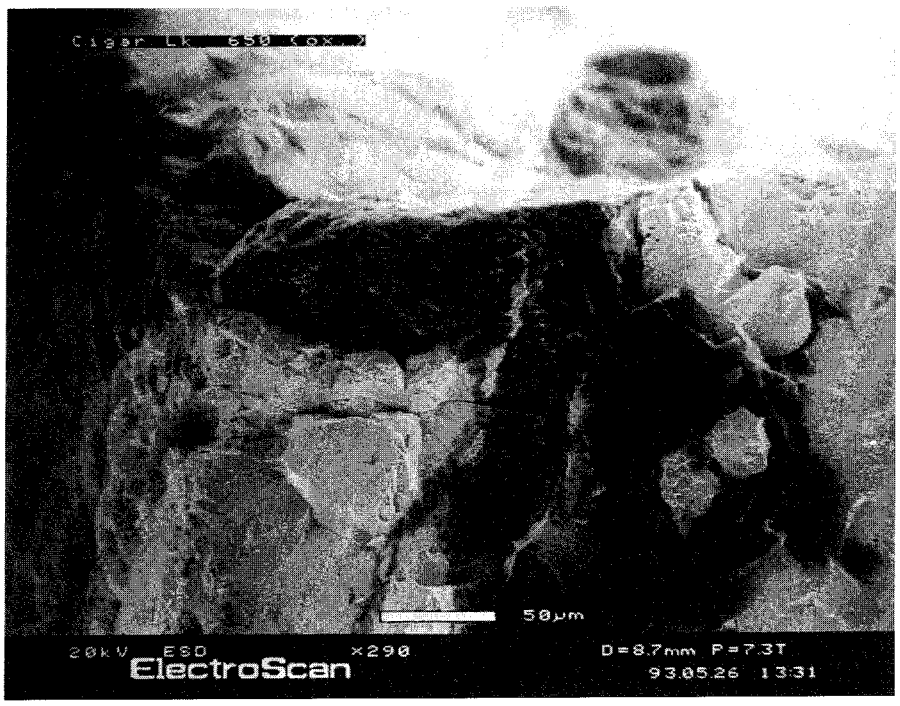

FIGURE 17. SEM image of the Cigar Lake sample leached under oxidizing conditions. Bright contrast areas are leached uraninite, the darker material with the textured surface is probably altered illite/chlorite, the darkest material is amorphous silica.

The surface appeared to be covered by a gel-like material. The surface composition was relatively uniform in U and Pb, with a significant amount of Fe present. The clay matrix, which remained physically intact, appeared to be chemically altered to Fe-oxide and unidentified Al-silicates. Substantial U was

also present in the clay matrix, although high concentrations were observed in some matrix clays of the unleached sample as well. Amorphous silica precipitated on the surface as a white crust during ESEM examination. The surface of the sample without the silica crust remained black (Figures 17 and 18).

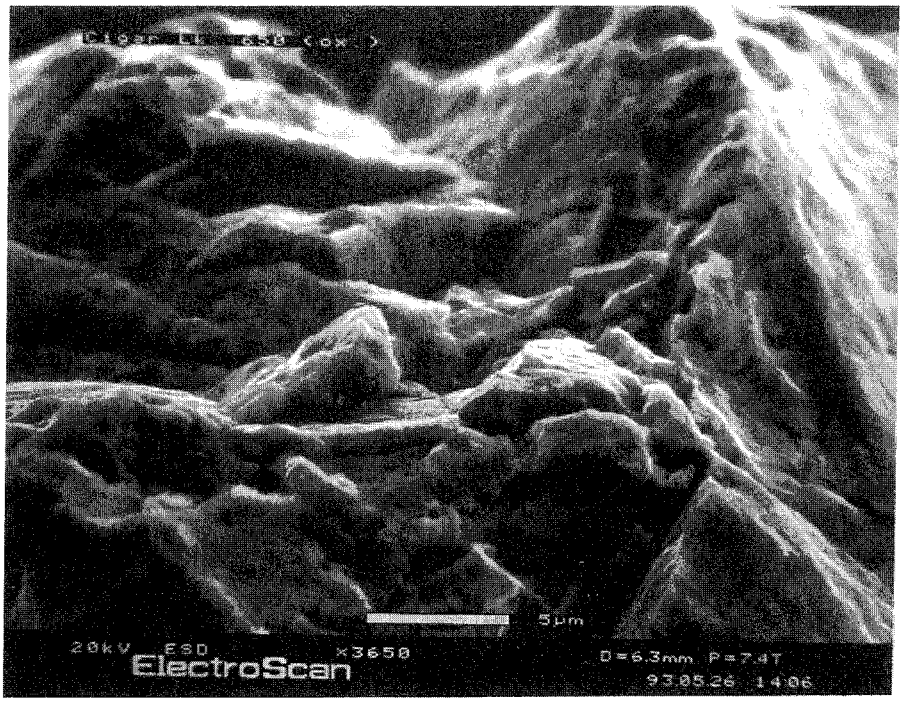

FIGURE 18. SEM image of the uraninite from Cigar Lake surface leached under oxidizing conditions, showing the gel-like layer on the surface.

Schoepite from Shaba, Zaire (#484)

This sample degraded only slightly over the course of the experiment to form some fine powder along with a single larger poly-crystalline grain.

The leached solid did not appear significantly different from the unleached one. It also contained minor becquerelite, and probably billietite and an unidentified Pb-uranyl oxide hydrate, not detected in the unleached material. These phases are commonly intergrown with schoepite. A few grains from the dried powder had fine-grained white material on the surface of the yellow schoepite that resembled rutherfordine.

Numerous schoepite grains appeared to be strongly corroded. These were in close proximity to unleached, well-formed, incipient schoepite crystals

(tabular and prismatic forms), probably precipitated from solution during the course of the experiment. No well-formed schoepite crystals were observed in the unleached material (Figures 19 and 20).

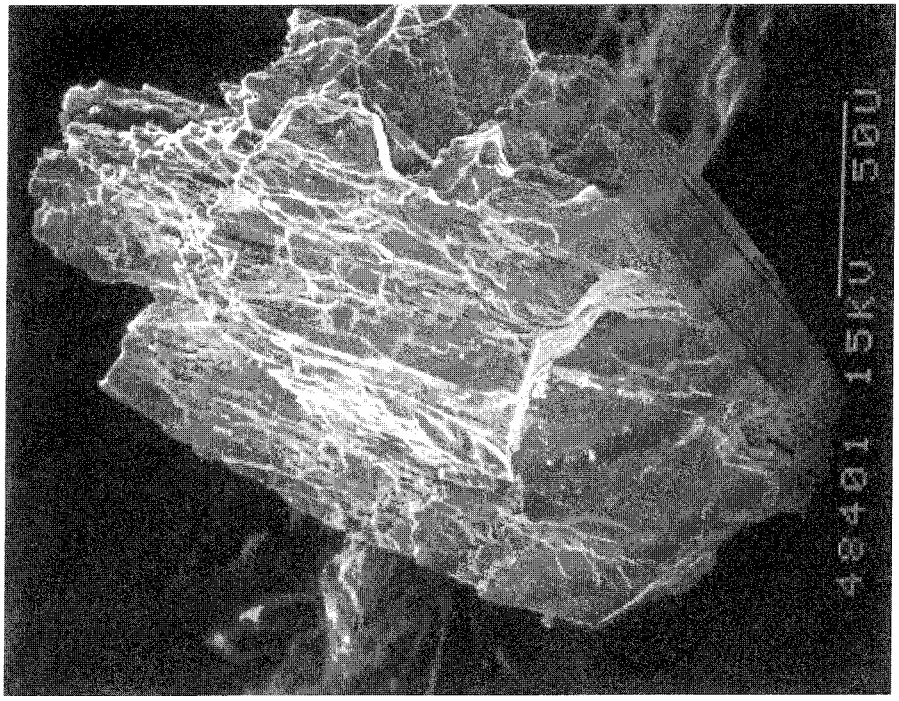

FIGURE 19. SEM image of the surface of schoepite particle after leaching which was allowed to dry overnight.

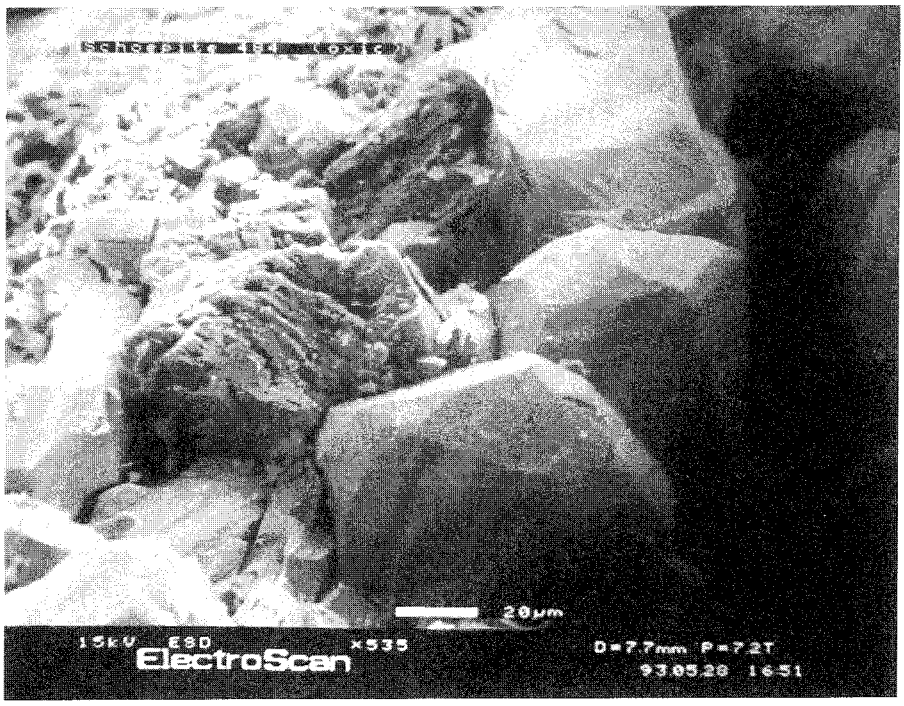

FIGURE 20. SEM image of euhedral, prismatic schoepite crystals, recently precipitated from solution, coexisting with corroded schoepite grains. Sample after leaching.

When the leached sample was returned to the solution, it floated. Dehydrated schoepite is hydrophobic and floats when initially added to water. A surface layer of dehydrated schoepite possibly formed during the ESEM analysis.

Uranophane from Shinkolobwe, Zaire (#548)

The leached material displayed some corroded grains, but most of the uranyl silicate crystals were pristine in appearance. Several uranyl silicate crystals were covered by a thin unidentified coating, but these were only observed in the SEM specimen and may be an artifact of sample preparation (Figures 21 and 22).

Ni-sklodowskite, soddyite and probably kasolite were identified like in the unleached material. Kasolite commonly has the same habit as the other uranophane group minerals, so that habit alone is not diagnostic.

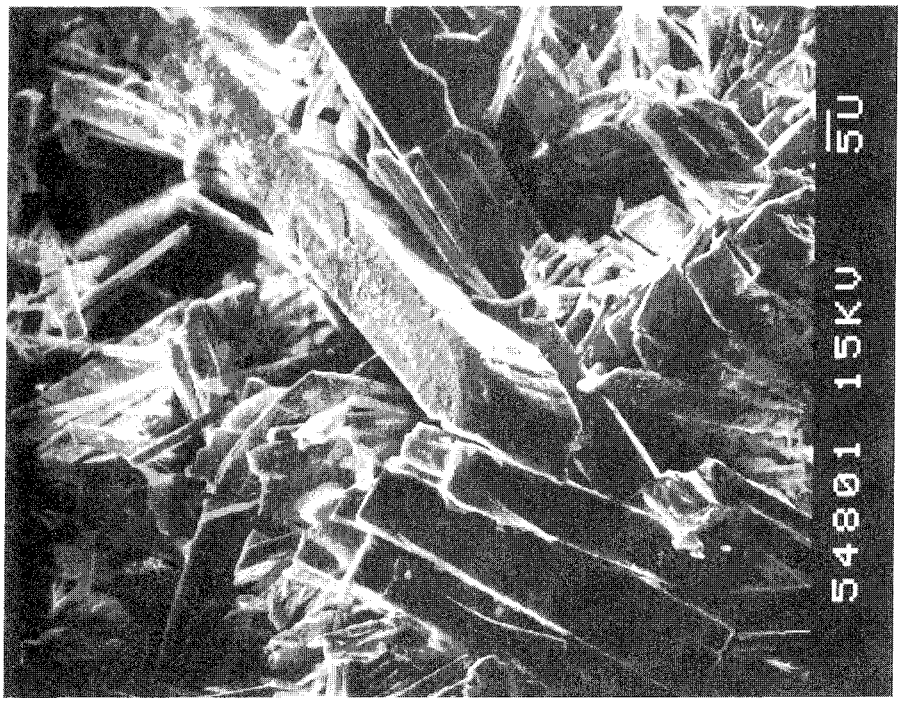

FIGURE 21. SEM image of leached uranophane crystals (#548), allowed to dry overnight.

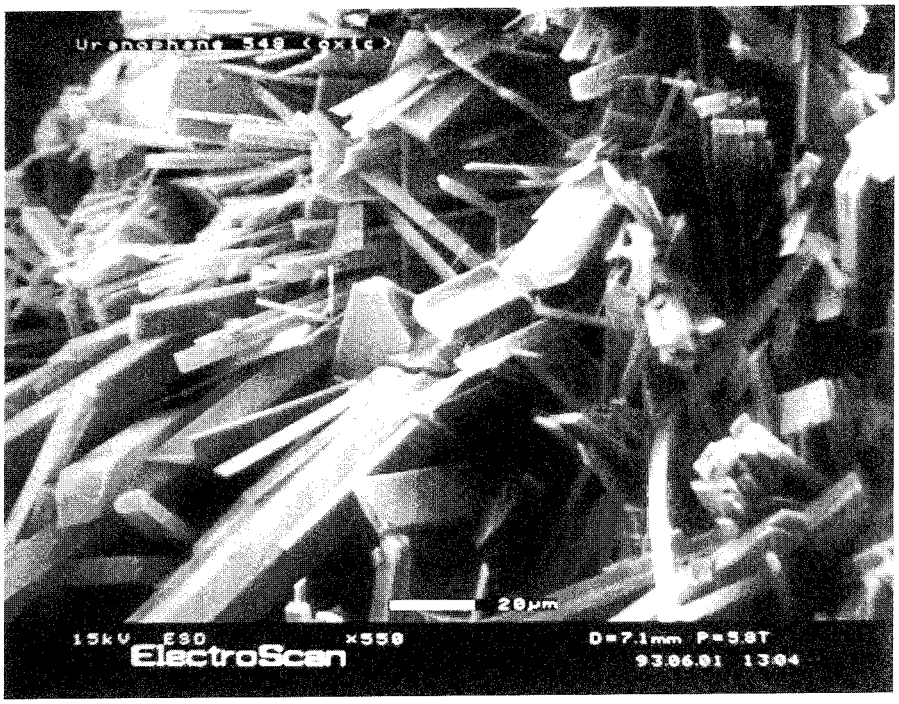

FIGURE 22. SEM image of uncorroded uranophane crystals (#548) on the surface.

Dissolution results

Uraninite solubility. Reducing conditions

The results obtained from the three different samples, Cigar Lake (650), Jachimov (430) and Oklo (690), are presented in figure 23.

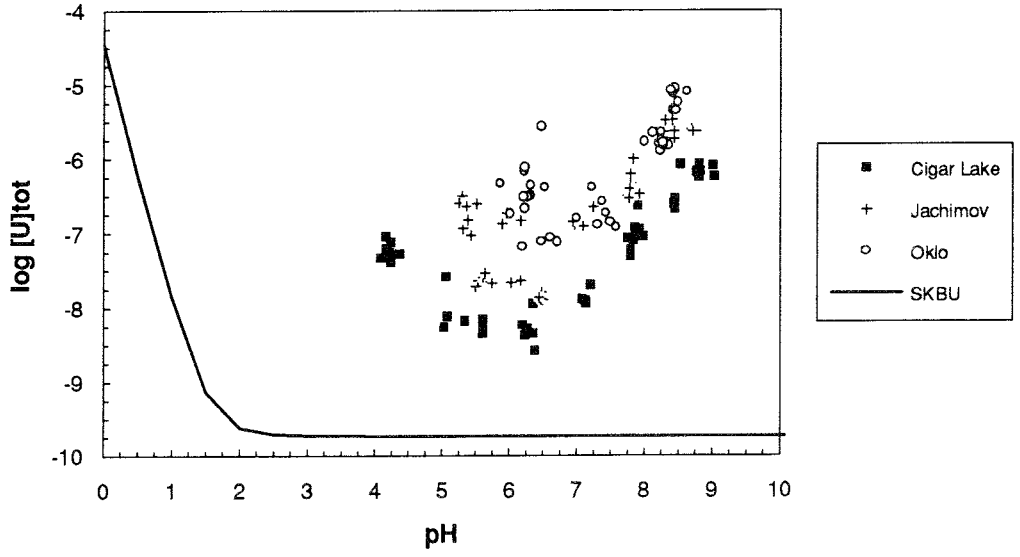

FIGURE 23

In this figure, we show for the three samples a similar pH dependence behavior of the total uranium concentration in solution under reducing conditions: a solubility increase at both relatively high and low pH values (compared to the SKBU model for $UO_2(c)$ under reducing conditions, shown as a full line in figure 23), with a minimum near pH 6. As seen in the figure, the experimental values cannot be modeled by considering only $UO_2(c)$ in equilibrium with the U(IV) aqueous complexes, and some additional considerations must be made to explain the experimental data.

In a first attempt, we thought on the possibility of some oxidation of U(IV) to U(VI) which would result in an increase of the solubility. In figures 24 and 25 we present the Pourbaix diagrams of uranium aqueous complexes and uranium solid phases, respectively, according to the database used. In figure 24 we have included and highlighted the line corresponding to the transition between $UO_2(c)$ and $U_4O_9(c)$, which shows that $UO_2(c)$ can still be predominant in equilibrium with U(VI) aqueous complexes at both low and high pH values.

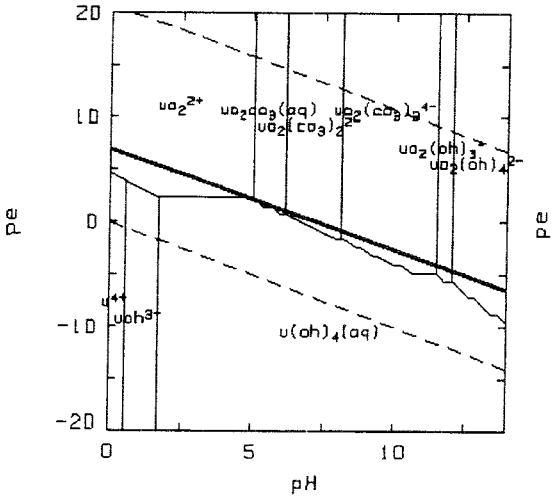

FIGURE 24

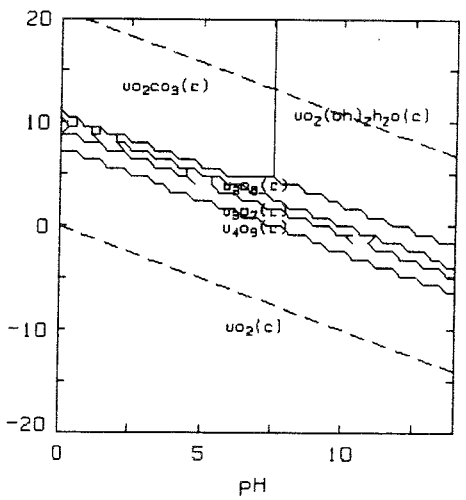

FIGURE 25

The presence of a certain amount of U(VI) in solution might explain the solubility increase found at both the low and high pH ranges, even considering that the solid phase remains practically unaffected. The solubility increase at alkaline values would be even higher in the presence of carbonate in the test solution, due to the formation of the highly stable U(VI)-carbonate complexes.

A preliminary modeling of the data has been done as follows. First of all, the effect of pe on the solubility has been checked, considering in this initial calculation that no carbonate is in solution (figure 26). As shown in this figure,

an increase of solubility is obtained at acidic pH values when increasing pe, as a consequence of augmenting the percentage of U(VI) in aqueous solution. A slight increase of the total uranium concentration at relatively high alkaline values is seen as well.

For a (pe+pH) = 7.25, the modeled values approached the experimental ones obtained between pH 4 and 4.5 for the uraninite from Cigar Lake (which is found to give the lowest uranium concentrations of the three samples). This pe range falls into the predominance zone of $UO_2(c)$, as can be observed in figure 4, reaching a maximum value for the equilibrium line between $UO_2(c)$ and $U_4O_9(c)$.

The pe value used to obtain the previous fitting was compared to the experimental redox determinations. As we mentioned in the experimental section, the redox potential was continuously monitored using a platinum wire. The pe values calculated from these measurements were compared with the corresponding pH determinations, and the following relationships were obtained:

Cigar Lake: $pH + pe = 4.0 \pm 0.7$

Jachymov: $pH + pe = 8.1 \pm 1.4$

Oklo: $pH + pe = 4.0 \pm 0.9$

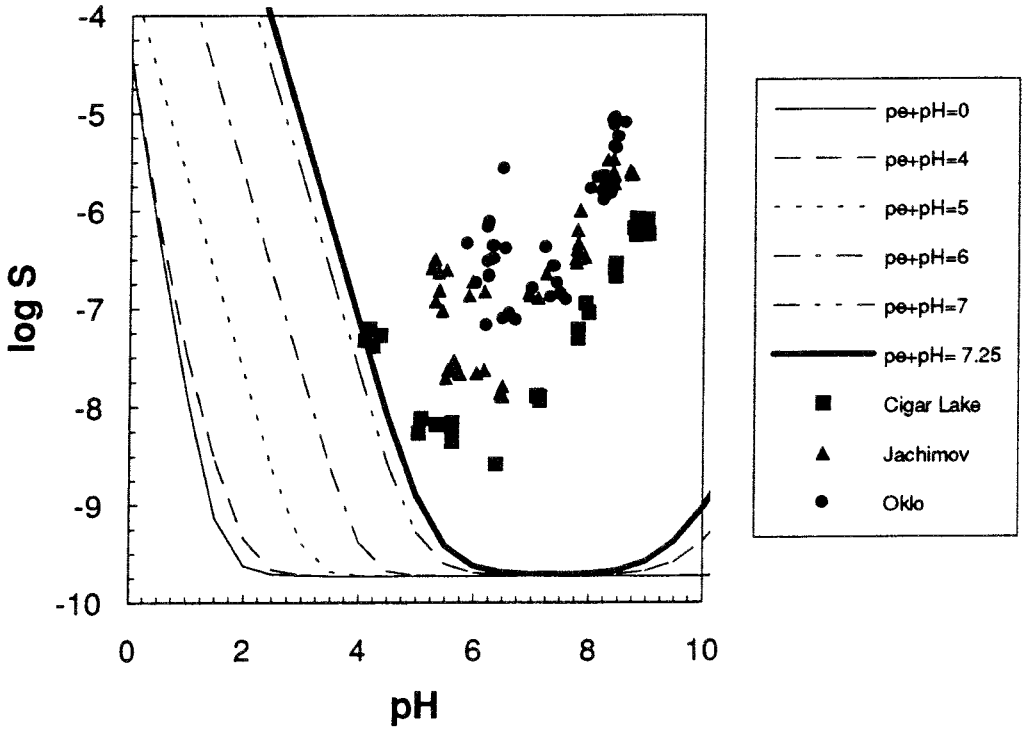

FIGURE 26

These experimental determinations are not far from the pe's used in the model of figure 26 (principally the ones obtained for Jachymov uraninite). Considering the inherent difficulties of the redox potential determinations, we conclude that it is experimentally demonstrated that we had relatively oxidizing conditions in the experiments, which supports the model presented. These high potentials are not surprising even if we consider the presence of hydrogen and the palladium catalyst. The characterization of the solid phase has unambiguously shown the high percentage of U(VI) in the natural samples. This leads to the presence in solution of some uranium(VI), and the U(IV)/U(VI) couple (either in solid or in aqueous phase) can buffer the redox potential leading to the relatively high determinations.

If we assume the presence of U(VI) in the aqueous phase, then the carbonate concentration in solution will play an important role as complexing agent, due to the formation of the stable U(VI)-carbonate complexes. We checked whether the increase of solubility at alkaline pH values could be explained by this complexation process. The pe values were fixed to the ones fitted above (pH+pe=7.25) and we steadily increased the carbonate concentration. The results are shown in figure 27.

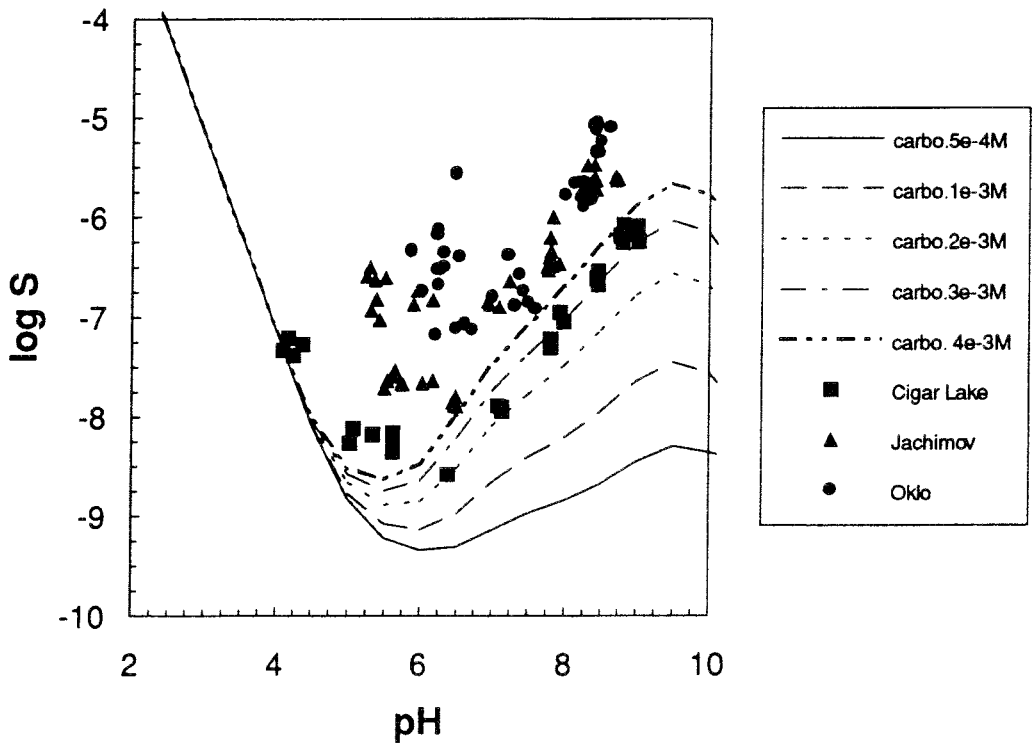

FIGURE 27

As is evident, a good fit to the data is found for a carbonate concentration of approximately 0.004 M, which corresponds to the actual carbonate concentration in the experiments. This increase of solubility at alkaline pH values could be the responsible of the sometimes assumed presence of a fifth anionic hydroxo complex of U(IV) claimed by some researchers and used in some of the uranium thermodynamic databases (Kraus and Nelson, 1955; Gayer and Leider, 1957; Baes and Mesmer, 1976; Lemire, 1988). This constant has been discarded, or found to be much less predominant than previously assumed, in some of the more recent uranium thermodynamic data compilations (Bruno and Puigdomènech, 1989, Grenthe et al., 1990). However, no explanation was yet available for the high uranium concentrations found in some experiments at alkaline pH values, which could be due to the presence of partial oxidation of the aqueous U(IV), combined with hydroxo and/or carbonate complexation.

As shown in figures 26 and 27, the system is extremely sensitive to small changes in both pe and total carbonate concentration. While the carbonate concentration in solution can readily be maintained constant throughout the experiments, we cannot ensure the same for the redox potential. This very sensitive parameter can be largely affected by an extremely low concentration of any oxidant species, particularly from the solid phase. The high sensitivity of the system to this parameter can certainly explain both the scatter of data found in our experiments, as well as the large range of solubilities found in the literature.

It is worth noting that the modeling was completed by using the solubility product constant found in the database for a well crystallized uranium dioxide. Many of the solubility experiments found in the literature do not fit this K_{s0} because experimental uranium concentrations are larger than expected. Generally, a better fitting is found using the solubility product constant defined as $UO_2(f)$ (Bruno and Puigdomènech, 1989), which is considered to be a less crystalline solid phase, which gives larger uranium concentrations.

As a final consideration, it must be taken into account the effect due to the different grain sizes of the samples, as well as the possibility of a readily release of uranium possibly sorbed on the clay fraction, which may likely influence on the total uranium determined in solution. These effects could, at least to some extent, account for the different solubilities observed for the three solid samples studied.

Becquerelite solubility. Anoxic conditions

Total uranium and calcium concentrations in solution as a function of pH are presented in figure 28. Calcium was also analyzed in some samples at higher pH values, but in those cases its concentration was found to be below the detection limit of the applied analytical technique. This experiment was completed in double distilled water under a continuous flux of nitrogen.

The dissolution reaction of this mineral can be written as:

$$Ca[(UO_2)_6O_4(OH)_6]\cdot 8H_2O_{(s)} + 14H^+ \Leftrightarrow Ca^{2+} + 6UO_2^{2+} + 18H_2O \qquad [1]$$

With a solubility product constant defined as:

$$K_{s0} = \frac{(a_{Ca^{2+}})(a_{UO_2^{2+}})^6(a_{H_2O})^{18}}{(a_{Ca[(UO_2)_6O_4(OH)_6]\cdot 8H_2O})(a_{H^+})^{14}} \qquad [2]$$

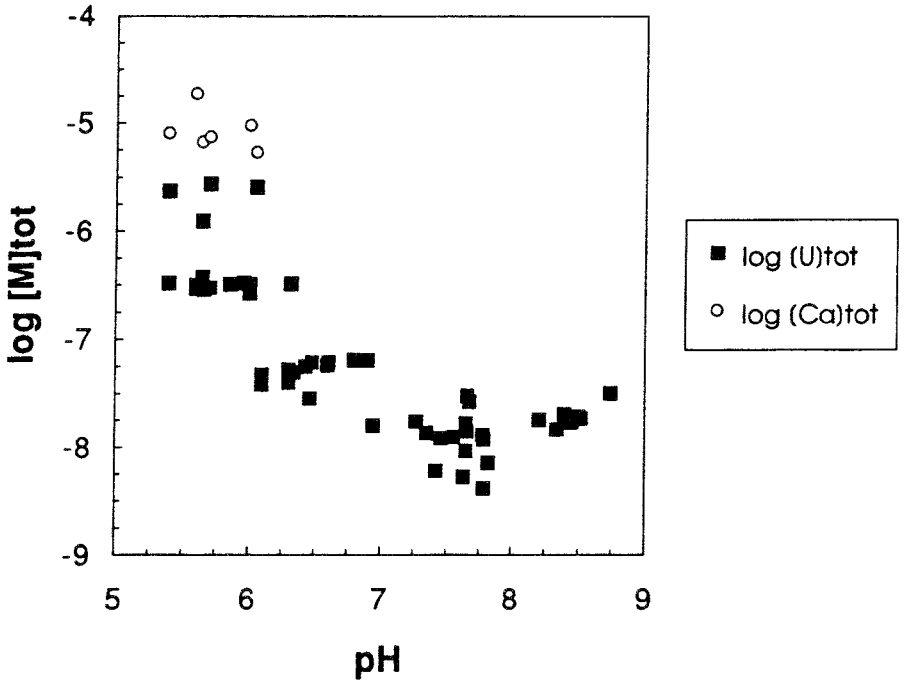

FIGURE 28

At the low concentrations of soluble species measured in these experiments and considering the objectives of the present work, we can assume that:

$$a_{Ca^{2+}} \approx [Ca^{2+}]$$

$$a_{UO_2^{2+}} \approx [UO_2^{2+}]$$

$$a_{H^+} \approx [H^+]$$

$$a_{H_2O} = a_{Ca[(UO_2)_6O_4(OH)_6]\cdot 8H_2O} \approx 1$$

Therefore:

$$K_{s0} = \frac{[Ca^{2+}][UO_2^{2+}]^6}{[H^+]^{14}}$$

[3]

Hereafter, this will be the expression that we will use when referring to this constant.

According to the stoichiometry of the dissolution reaction, the congruent dissolution of becquerelite in water should give a total uranium concentration in solution of six times the total calcium concentration. Then, if we define the calcium concentration as the solubility (s) of the solid phase, the total uranium concentration in solution should be equal to 6s.

On the other hand, since the test solution does not include any other complexing agent than hydroxide, we can write:

$$[U]_{tot} = [UO_2^{2+}] + [UO_2OH^+] + [UO_2(OH)_2] + [UO_2(OH)_3^-] + [UO_2(OH)_4^{2-}] + \\ + 2\cdot[(UO_2)_2OH^{3+}] + 2\cdot[(UO_2)_2(OH)_2^{2+}] + 3\cdot[(UO_2)_3(OH)_4^{2+}] + \\ + 3\cdot[(UO_2)_3(OH)_5^+] + 3\cdot[(UO_2)_3(OH)_7^-] + 4\cdot[(UO_2)_4(OH)_7^+]$$

[4]

This expression can be rewritten as:

$$[U]_{tot} = [UO_2^{2+}]\cdot A + 2\cdot[UO_2^{2+}]^2\cdot B + 3\cdot[UO_2^{2+}]^3\cdot C + 4\cdot[UO_2^{2+}]^4\cdot D$$

[5]

where:

$$A = 1 + \frac{\beta_{11}}{[H^+]} + \frac{\beta_{12}}{[H^+]^2} + \frac{\beta_{13}}{[H^+]^3} + \frac{\beta_{14}}{[H^+]^4}$$

$$B = \frac{\beta_{21}}{[H^+]} + \frac{\beta_{22}}{[H^+]^2}$$

$$C = \frac{\beta_{34}}{[H^+]^4} + \frac{\beta_{35}}{[H^+]^5} + \frac{\beta_{37}}{[H^+]^7}$$

$$D = \frac{\beta_{47}}{[H^+]^7}$$

[6]

being β_{ij} the constants of formation of the corresponding uranium(VI)-hydroxo complexes.

In the next step, the free uranyl ion concentration in equation 5 is expressed, according to equation 3, as a function of the solubility product constant and the calcium concentration (s):

$$[UO_2^{2+}] = (K_{s0} \cdot [H^+]^{14} / s)^{1/6}$$

[7]

Finally, substituting in equation 5 the total uranium concentration by 6s and using the complex formation constants (β_{ij}) found in the SKB uranium database (SKBU), we can solve the equation for the solubility (s) as a function of pH for a given solubility product constant value:

$$6s = (K_{s0}[H^+]^{14} / s)^{1/6} \cdot A + 2 \cdot (K_{s0}[H^+]^{14} / s)^{1/3} \cdot B + 3 \cdot (K_{s0}[H^+]^{14} / s)^{1/2} \cdot C + \\ + 4 \cdot (K_{s0}[H^+]^{14} / s)^{2/3} \cdot D$$

[8]

Graphical treatment

A systematic comparison of the theoretical function with the experimental data gave a visually determined best fit for a log K_{s0} of 30.5±1.0. The comparison between the calculated solubilities and the experimental data is shown in figure 29.

This solubility constant, differs from the previously published value of 43.6 (Vochten and Van Haverbeke, 1990). Their work was based on the determination of the calcium concentration in solution once equilibrium was assumed. Using this value, the experimentally measured pH, the stoichiometry of the solid phase and the constants of formation of the U(VI)-hydroxo complexes, the free uranyl ion concentration was deduced and the solubility product constant calculated according to equation 3.

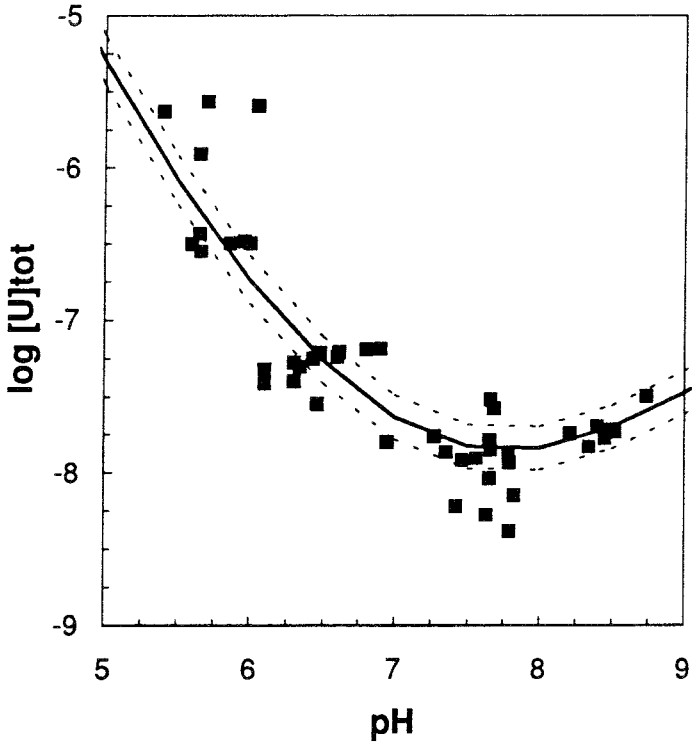

FIGURE 29

In our study, we also determined the calcium concentration in a few samples, as seen in figure 28. In those cases calcium was found at a higher concentration than should be expected from congruent dissolution, according to the uranium values. Either the dissolution and/or the formation of a secondary solid phase could explain the incongruency between U and Ca, since the solid characterization showed evidence of other solid phases, i.e., uranophane. A hypothetical mechanism of dissolution of this solid phase and precipitation of, for instance, soddyite, would result in an excess of calcium respect to the uranium content, according to the following reaction:

$$Ca[(UO_2)(SiO_3OH)]_2 \cdot 5H_2O_{(s)} \Leftrightarrow (UO_2)_2SiO_4 \cdot 2H_2O_{(s)} + Ca^{2+} + H_4SiO_4 + 3H_2O \quad [9]$$

To test the possibility of having the aqueous solution equilibrated with a solid phase different than becquerelite, we compared the experimental data to the calculated solubility curves of uranophane, soddyite and schoepite, which we considered the most likely secondary phases to be formed. The comparison is shown in figure 30. None of the models was found to fit the experimental data for the whole pH range studied. The comparison of these models with the one presented in figure 29, made us to conclude that our dissolution results are most likely to correspond to becquerelite.

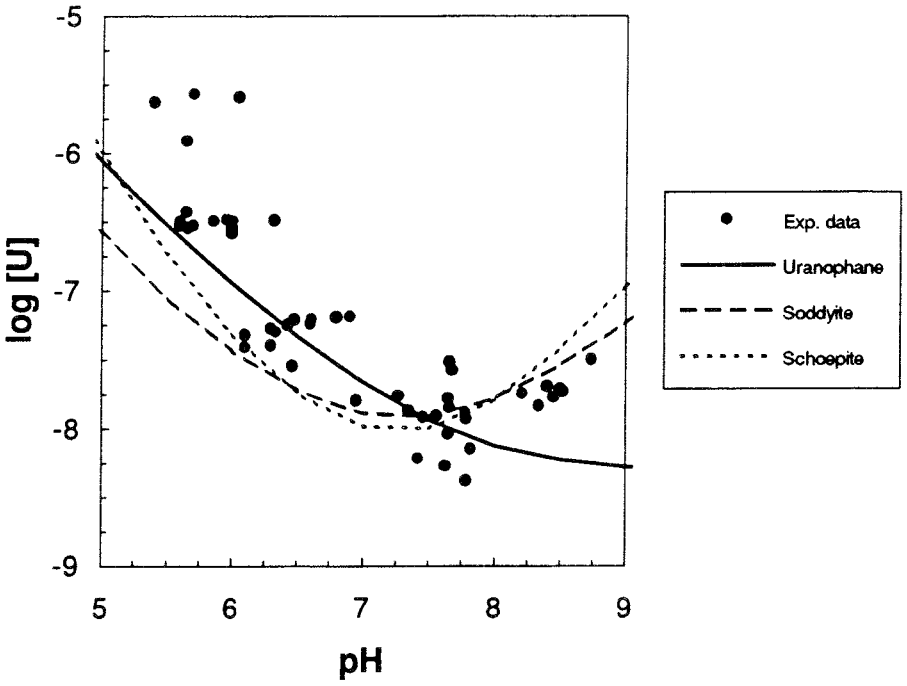

FIGURE 30

On the other hand, the calcium concentrations were found to correspond quite well with those measured by Vochten (Vochten and Van Haverbeke, 1990). However, since in our case we have not only the calcium determinations but also the corresponding uranium values, we can calculate the free uranyl ion concentration from the total uranium determinations, and not from the calcium values as in Vochten's paper. In this way, we avoid errors that may arise due to noncongruent dissolution processes.

The calculation of the free uranyl ion concentration was made by using equation 5 and the experimental pH values. From the available series of values of $[UO_2^{2+}]$, $[Ca^{2+}]$ and $[H^+]$, we calculated the solubility product constant according to equation 3. The value obtained was:

$$\log K_{s0} = 32.7 \pm 1.3$$

which is somewhat larger than the one used in the previous fit (figure 29), but it is still much lower than the value found in the literature. We have considered this result as an upper limit for the solubility product constant of becquerelite.

The main conclusion that arises from these calculations is that becquerelite is more stable than was previously assumed. The uranium concentrations measured are lower than any other values determined for an oxy-hydroxy

U(VI) solid phase. In fact, the levels of uranium in solution are closer to the solubility of some U(IV) solid phases than are to U(VI) compounds of the same type.

By using the solubility product determined in this work for becquerelite together with the solubility product of schoepite (log K_{so}=5.58) selected in the SKB uranium database (Bruno and Puigdomènech, 1989) we have drawn figure 31. This solubility product of schoepite coincides with the ones given by Langmuir (Langmuir, 1978) (selected in the CHEMVAL 2 database compilation) and by Lemire and Tremaine (Lemire and Tremaine, 1980) of 5.5 and 5.6, respectively. On the other hand, this value is somewhat higher than the one selected in the NEA uranium database (Grenthe et al., 1990) of 4.82, while, it is lower than the ones determined by Sandino and Bruno (Sandino and Bruno, 1992) for an amorphous and a crystalline solid phase, of 6.33 and 5.97, respectively.

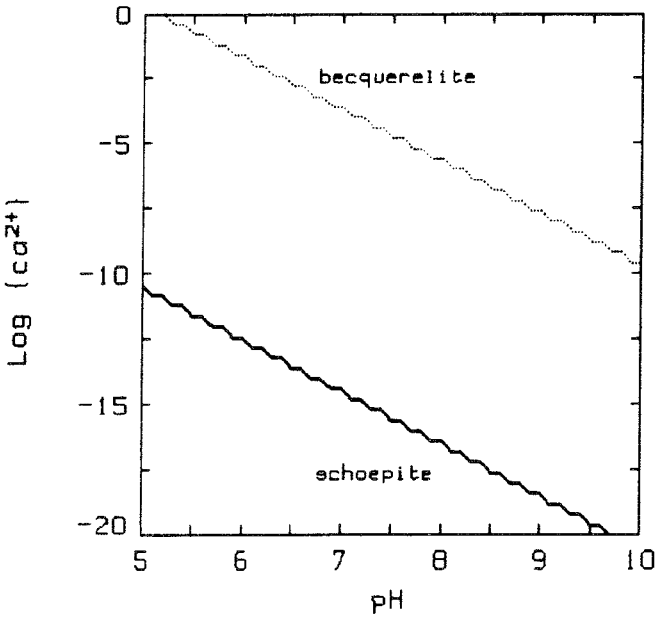

FIGURE 31

Two different areas of predominance are evident. In one case the equilibrium between becquerelite and schoepite is calculated with the constant presented in this work (solid line in figure), and in the second case it is calculated with the value found in the literature (Vochten and Van Haverbeke, 1990) (dotted line). Becquerelite is a much more stable phase than schoepite under the pH conditions expected in a granitic repository, even at very low calcium concentrations. There are several observations, both in nature and in laboratories, that have already shown that the schoepite initially formed under oxidizing conditions (perhaps due to either a more favored kinetics of

formation or to the lack of calcium ions), when put in contact with a calcium containing solution leads after some time to the formation of becquerelite, even at low temperatures (Vochten and Van Haverbeke, 1990; Sandino and Grambow, pers. commun.).

A recent study by Sandino and Grambow (personal communication) on the solubility of becquerelite in a 1 molal $CaCl_2$ solution does not seem to correspond to the results of this work. They obtained higher total uranium concentrations in solution, which is inconsistent with our data, considering their 1 molal calcium concentration in solution. This high concentration of a common ion should, in principle, result in lower solubilities. Although at this point a more careful investigation of the data and procedures must be made, an initial explanation may be differences in the degree of cristallinity of the solid phases, comparing their synthetically prepared becquerelite to our well crystallized natural becquerelite.

Uranophane solubility. Anoxic conditions

Three different experiments were carried out with this uranium phase under anoxic conditions, as explained in the experimental section: two of them in polyethylene bottles (uranophane solid samples 514 and 655), while the third one was done in a glass vessel (sample 446). In all cases we used double distilled water as test solution. In order to avoid an unnecessary complexity, we have plotted separately the uranium data (figure 32) and the corresponding Ca and Si (figure 33) determined in the two polyethylene vessels.

The dissolution reaction of this solid phase is described by the following reaction:

$$Ca[(UO_2)(SiO_3OH)]_2 \cdot 5H_2O_{(s)} + 6H^+ \Leftrightarrow Ca^{2+} + 2UO_2^{2+} + 2H_4SiO_4 + 5H_2O \quad [10]$$

This implies that, in this case, the total concentrations in solution of calcium, uranium and silicon, will follow the ideal proportions 1:2:2, respectively, assuming a congruent dissolution behavior. Then, we will identify the total calcium as the solubility (s), the total uranium as twice the solubility (2s), and the same for the total silicon (2s).

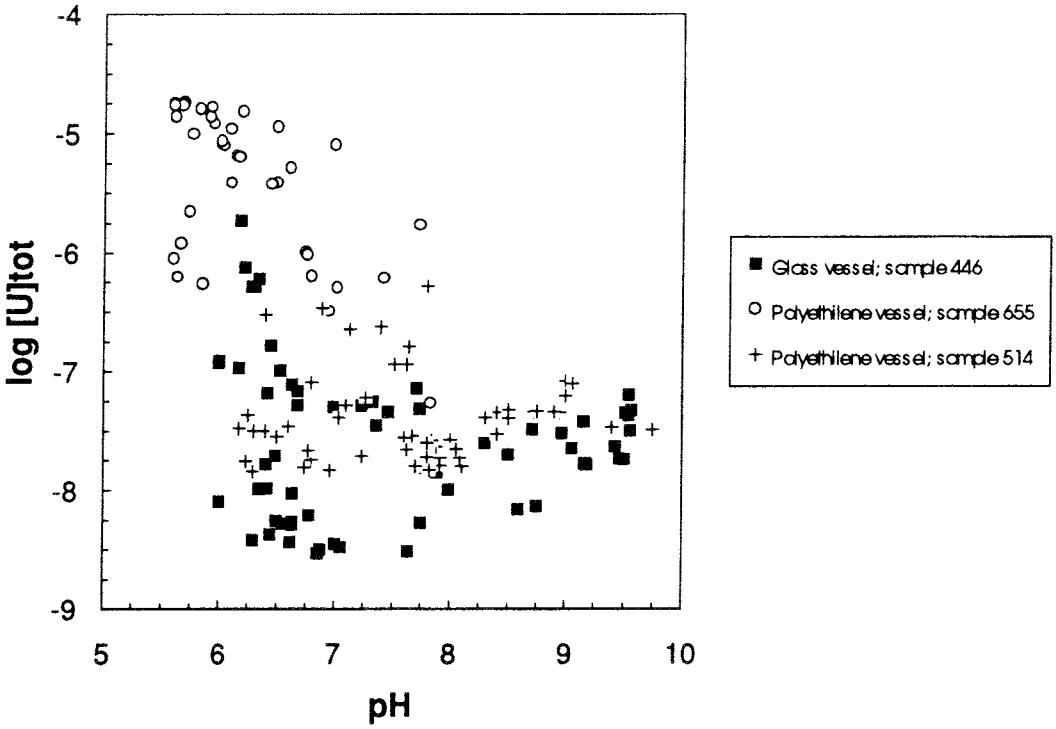

FIGURE 32

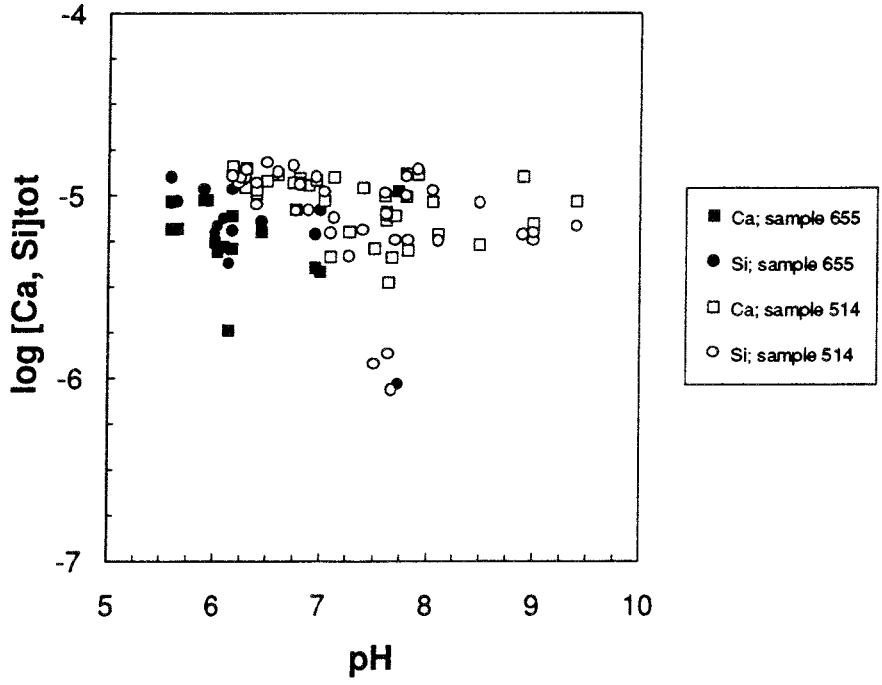

FIGURE 33

We define the solubility product constant (based on the same considerations used for becquerelite, equation 3) as:

$$K_{s0} = \frac{[Ca^{2+}][UO_2^{2+}]^2[H_4SiO_4]^2}{[H^+]^6} \qquad [11]$$

Then, we can express the free uranyl ion concentration as:

$$[UO_2^{2+}] = \sqrt{\frac{K_{s0} \cdot [H^+]^6}{4s^3}} \qquad [12]$$

where $4s^3$ is the product $[Ca^{2+}][H_4SiO_4]^2$.

In equation 5, we can now substitute the total uranium concentration by 2s and the free uranyl concentration by equation 11, and solve the resulting expression to obtain s values as a function of pH, for a given solubility product constant. The calculated values were systematically compared to the experimental data for different values of K_{s0}. The trend of the calculated solubilities did not quite follow the behavior of the experimental uranium data, as shown in figure 34. The calculated uranophane solubility is shown as a full line. The constant used to obtain the model was:

$$\log K_{s0} = 6.5$$

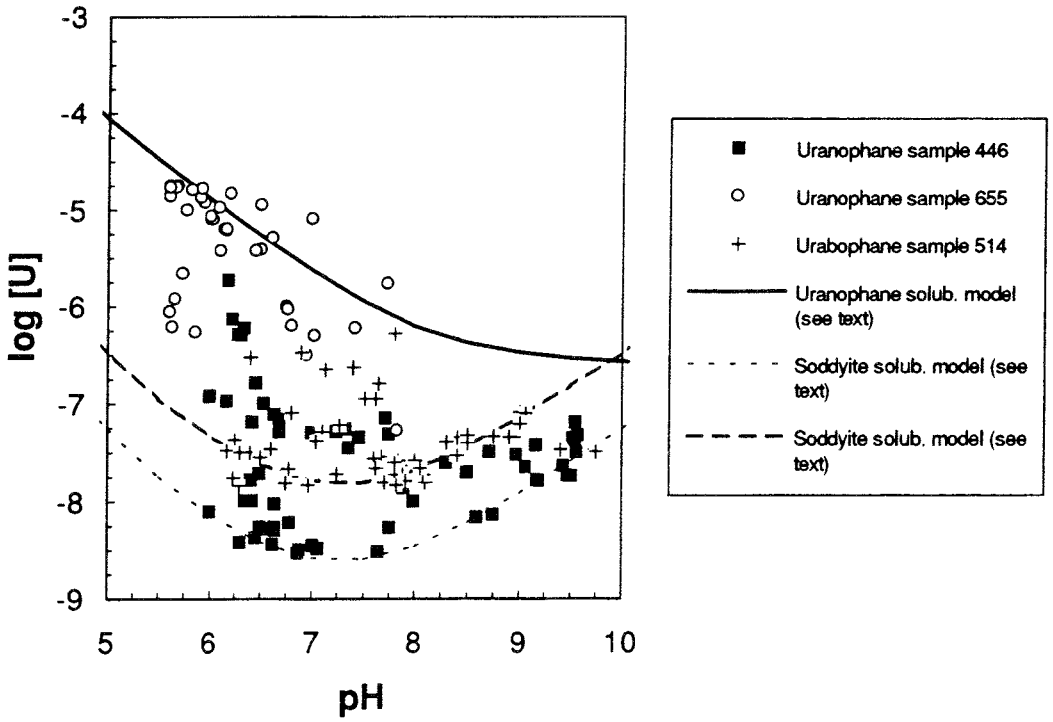

FIGURE 34

As shown in the figure, we selected the model that was closer to the highest uranium concentrations determined. In this way, the K_{s0} represents a conservative value. The experimental data correspond to one of the experiments carried out in a polyethylene vessel (uranophane solid sample 655). In some of the aqueous samples of this experiment, Ca and Si were also determined. The ratios between the three elements for these samples were:

$$Ca : U : Si$$

$$1 : 1.74(\pm 0.79) : 1.43\pm(0.38)$$

In contrast with the ideal stoichiometric ratios of:

$$1 : 2 : 2$$

or with the ones determined in the chemical characterization of:

$$0.89 : 2.12 : 1.88$$

This implies a stoichiometric excess of Ca in solution (as in the previous case for becquerelite), or U and Si depletion. Anyway, this experiment was the one giving the closest to ideal Ca:U:Si ratios. Then, we used it to calculate the K_{s0} from the corresponding $[UO_2^{2+}]$, $[Ca^{2+}]$ and $[H_4SiO_4]$ in solution, where the free uranyl concentration was calculated as described for becquerelite.

The value we obtained was:

$$\log K_{s0} = 7.8 \pm 0.8$$

which, again, and due to the non stoichiometric ratios, gives a solubility product constant higher than the one determined above. We consider this value as an upper limit for the solubility product constant of our sample. Although, this value is still lower than the one found in the literature of 9.42± 0.48 (Nguyen et al., 1992), concluding at this point that our natural uranophane sample is thermodynamically more stable than literature values (determined from synthetic materials) would indicate.

The lower uranium concentrations found for the other two experiments (solid sample 446 in a glass vessel and solid sample 514 in a polyethylene vessel), led us to consider the presence of a different solid phase as being responsible for the solubilities obtained. In this sense, the solid phase characterizations showed that uranophane was found in one case (solid sample 514, uranophane from Nisto Mines) associated to soddyite.

Therefore, we calculated the solubility that we would expect from this solid phase.

The dissolution of soddyite is described by the following reaction:

$$(UO_2)_2SiO_4 \cdot 2H_2O + 4H^+ \Leftrightarrow 2UO_2^{2+} + H_4SiO_4 + 2H_2O \quad [13]$$

With a solubility product constant of:

$$K_{s0} = \frac{[UO_2^{2+}]^2[H_4SiO_4]}{[H^+]^4} \quad [14]$$

and a corresponding free uranyl ion concentration of:

$$[UO_2^{2+}] = \sqrt{\frac{K_{s0} \cdot [H^+]^4}{s}} \quad [15]$$

where s in this case is the H_4SiO_4 total concentration.

Again, we substitute this expression in equation 5 and the total uranium concentration by 2s, and we calculate s values as a function of pH for a given solubility product constant.

The best fits considered are those presented in figure 34 as a dotted line, for data obtained in the glass vessel (446), and as a dashed line, for data collected in the polyethylene bottle (514). Neither the thermodynamic model found for uranophane nor the ones presented for soddyite can be considered a good fit to the experimental data.

However, such a thermodynamic model is not possible if we assume that the solid phase is changing its composition during the experimental time. In figure 35, the uranium concentrations corresponding to the experiment carried out with solid sample 514 in a polyethylene bottle, are plotted in the same sequential order as we collected the samples.

Interestingly, there is a clear trend of decreasing uranium concentrations with the experimental time. The highest values correspond to the samples that were taken at the very beginning of the experiment. The successive samples, show decreasing concentrations until they fall approximately on the above calculated soddyite solubility, shown as a solid line.

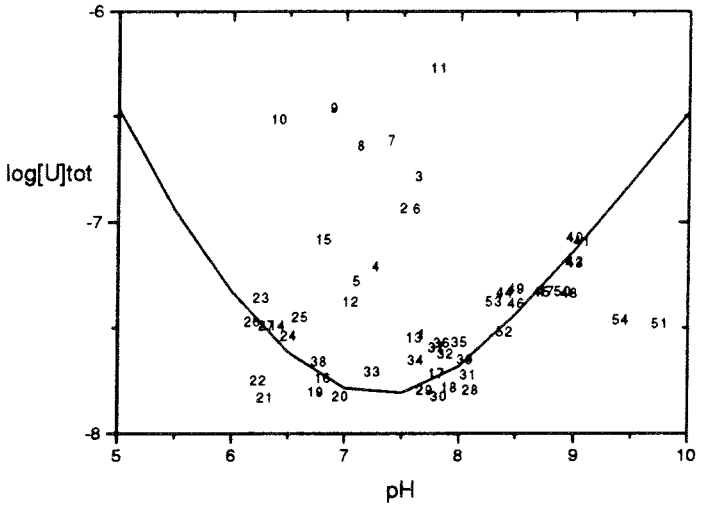

FIGURE 35

Thus, one can calculate upper limits that bracket the solubilities experimentally determined. For soddyite, we selected the model that is in good agreement with the data determined for solid sample 514 (Nisto Mines). In this experiment we obtained higher uranium concentrations than the ones determined in a glass vessel (446) (see figure 34). There is the possibility of silica leaching from the glass walls, which would lower the solubility of the solid phase considered. For this reason, data obtained in the polyethylene bottle seem to give both more realistic and conservative values.

The solubility product constant used for that model fit is:

soddyite: $\log K_{s0} = -0.2$

In these experiments, we also determined Ca and Si in several samples. In this case the ratio between Ca/Si and U are far from the ideal stoichiometric ratios, with uranium concentrations much lower than the expected values. In the experiment started with the uranophane sample from Nisto Mines (514), soddyite was positively identified in the final spectroscopic characterizations as having formed during the dissolution process.

The solubility product constant of soddyite was calculated from this experiment using the UO_2^{2+} and the H_4SiO_4 concentrations. The value obtained was:

$$\log K_{s0} = 3.0 \pm 2.9$$

Clearly, the uncertainty of this determination is too large to give a reliable value. Most of the samples probably do not correspond to equilibrium, due to the slow kinetics of solid phase transformation. However, we believe that this

value brackets the true solubility constant, because the formation of this new phase has clearly shown the tendency to result in lower uranium concentrations in solution. The constant given above, even with its associated large uncertainty, should lead to realistic predictions of the U concentrations under long term oxidizing weathering conditions.

This value was compared to the one determined by Nguyen et al. (Nguyen et al., 1992) of 5.74±0.21, obtained from a synthetic solid phase, and this is consistent with the maximum limit assumed for the constant presented in this work.

Even considering the large uncertainty of our defined constant, it is clear that the solubility product determined indicates a higher stability of the solid phase than previously assumed.

The differences in the predominance diagrams of uranium solid phases is shown in figures 36 and 37, where we have considered the presence of schoepite, becquerelite, uranophane and soddyite at a fixed pH of 8 (representative of a granitic groundwater), varying both calcium and silicon concentrations. In the figure at left, we used the following constants found in the literature, as described above:

schoepite:	$\log K_{s0} = 5.58$
becquerelite:	$\log K_{s0} = 43.6$
uranophane:	$\log K_{s0} = 9.42$
soddyite:	$\log K_{s0} = 5.74$

At the right (figure 37), we present the diagram made using the constants calculated in the present work, except for schoepite, for which we used the value given above:

becquerelite:	$\log K_{s0} = 32.7 \pm 1.3$
uranophane:	$\log K_{s0} = 7.8 \pm 0.8$
soddyite:	$\log K_{s0} = 3.0 \pm 2.9$

The dotted lines in the figure at right show the effect of the uncertainties of the constants in the predominance areas. As a solid line we show the result of using the mean constant values. The solid dot inside the uranophane predominance area, approximately shows the calcium and silicon concentrations corresponding to the groundwater composition selected in SKB 91 as reference case.

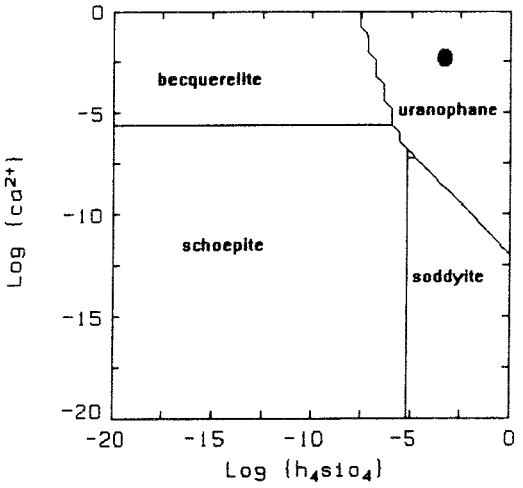

FIGURE 36

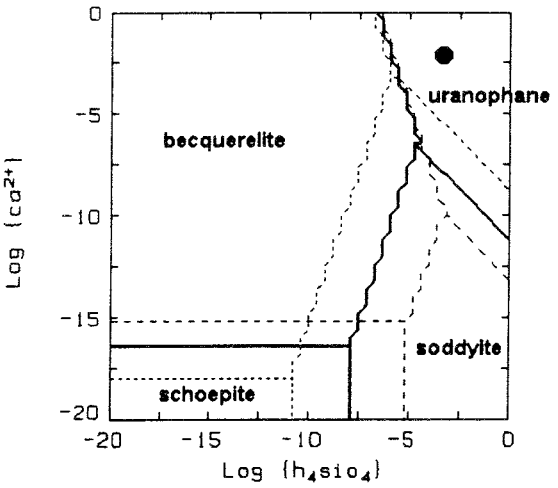

FIGURE 37

Notice the dramatic change in the area of predominance of becquerelite with respect to schoepite. As we found in the present work, becquerelite appears more stable than was previously assumed, and the predominance of schoepite is restricted to waters with very low calcium content. The transformation of schoepite into becquerelite in the presence of calcium has been extensively observed to occur even at low temperatures (Vochten and Van Haverbeke, 1990; Sandino and Grambow, pers. commun.).

The effect of silicon concentration, on the other hand, is poorly defined. The equilibrium between schoepite and soddyite fluctuates as much as five orders of magnitude, from a silicon concentration of 10^{-11} up to 10^{-5} M. The same poor definition is found in the thermodynamic limits between soddyite and uranophane, depending in this case of both calcium and silicon concentrations. These large ranges of uncertainty come from the poor definition of the soddyite solubility product.

However, even considering this large uncertainty, the groundwater composition selected in SKB 91 as reference case, clearly falls into the predominance area of uranophane for all cases considered.

In figure 38, we have excluded the uncertainty on both becquerelite and uranophane solubility constants to concentrate on the value corresponding to the soddyite (solid and dashed lines). We have also added to the figure the pairs of Ca-Si values determined in our experiments. It must be taken into account that the pH is not the same in all cases, although as it was seen in figure 33, this parameter does not effect significantly the calcium and silicon determinations. In the same figure, in dotted lines, are the predominance zones according to the literature values.

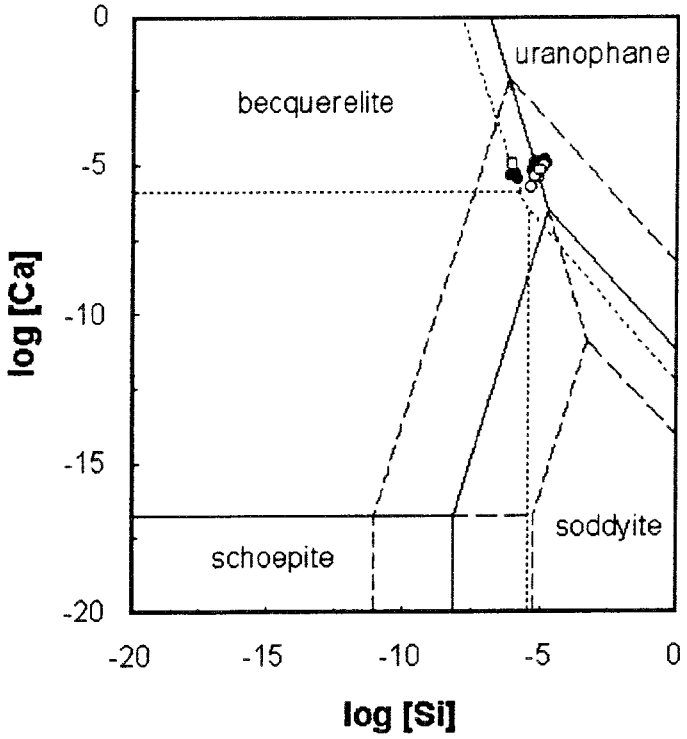

FIGURE 38

The interpretation of our results differs quite a lot depending on the solubility constant used. If we use the log K_{so} of 3.0 for soddyite, or the maximum of 3.0+2.9, we observe that the determined Ca and Si pairs of values fall in what should be close to the equilibrium between becquerelite and uranophane, and this should be the final solid phase in our experiment. However, if we use the log K_{so} of 3.01-2.92, then the pairs of data would fall into the predominance zone of soddyite, and we should observe the formation of this solid phase.

Finally, by using the values in the literature (dotted line) already given above, we should be moving between the becquerelite/uranophane equilibrium zone and the clear predominance of uranophane. Based on these constants, soddyite should not predominate under any of our experimental conditions.

We must recall that soddyite was clearly identified in one of the experiments (514), but not on the other two. It is clear that our system appears to be in the phase transition between becquerelite, uranophane and soddyite. Therefore, slight changes of the solution composition may favor the formation of either soddyite or uranophane.

As a final observation, in one of the experiments with uranophane (sample #655), the characterization of the solid phase pointed to the formation of some schoepite. The schoepite may have precipitated after the sample was

taken out of the test solution and before the characterization was made. Some crystals apparently formed during the experiment. However, this sample was initially quite complex, containing 10% vol. of soddyite and some schoepite as well. From the predominance diagram constructed with the constants determined in this study, schoepite should not have formed under these experimental conditions. The final question is whether, as already noted, we face a kinetic process, in which schoepite is initially formed and would subsequently transform to becquerelite.

The behavior that remains unexplained is that of both calcium and silicon. These two components of uranophane are dissolved to a larger extent than uranium. Trying to determine a mechanism of dissolution that could explain the experimental results, we studied the kinetic behavior of the system for the first 5000 hours. We present again the results in separate figures, uranium (Figure 39) and Ca and Si (Figure 40), due to the difference in concentration levels between these elements.

The trend of the uranium determinations indicates an initial dissolution followed by the subsequent precipitation of a less soluble solid phase, reaching a final value of equilibrium or steady state after 2000 hours. Whereas, Ca and Si follow an almost perfectly congruent dissolution behavior, both reaching equilibrium or steady state after 3000 hours.

The initial characterization of the solid phase indicated that it contained a large amount of quartz (50% by volume). However, Si release cannot solely be due to the leaching of quartz. The solubility limit of quartz was not attained, although this fact could be explained in terms of a source-controlled release. The main observation that points to a different phase as controlling the release of Si is the congruency between Ca and Si. In the long run, it was observed that changes in pH affected the concentration of both elements to the same extent. These experimental observations dismissed the hypothesis of $SiO_2(s)$ being responsible for the Si concentrations and led one to consider uranophane as being responsible of the behavior of these two elements. On the other hand, the final characterization of the solid phase unambiguously showed the formation of crystals of soddyite, which were not present in the unleached sample. The formation of soddyite could control the low uranium determinations.

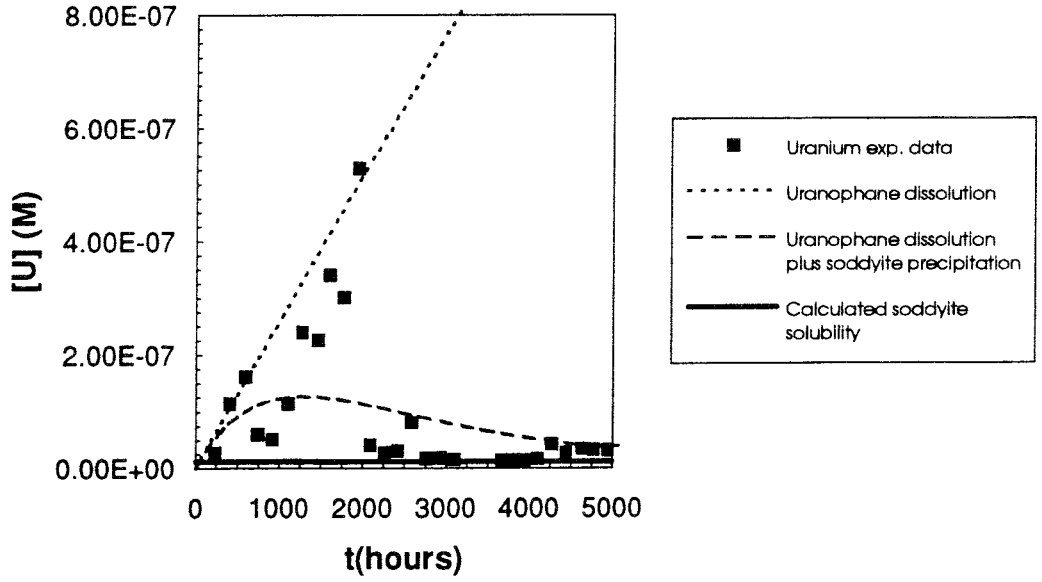

FIGURE 39

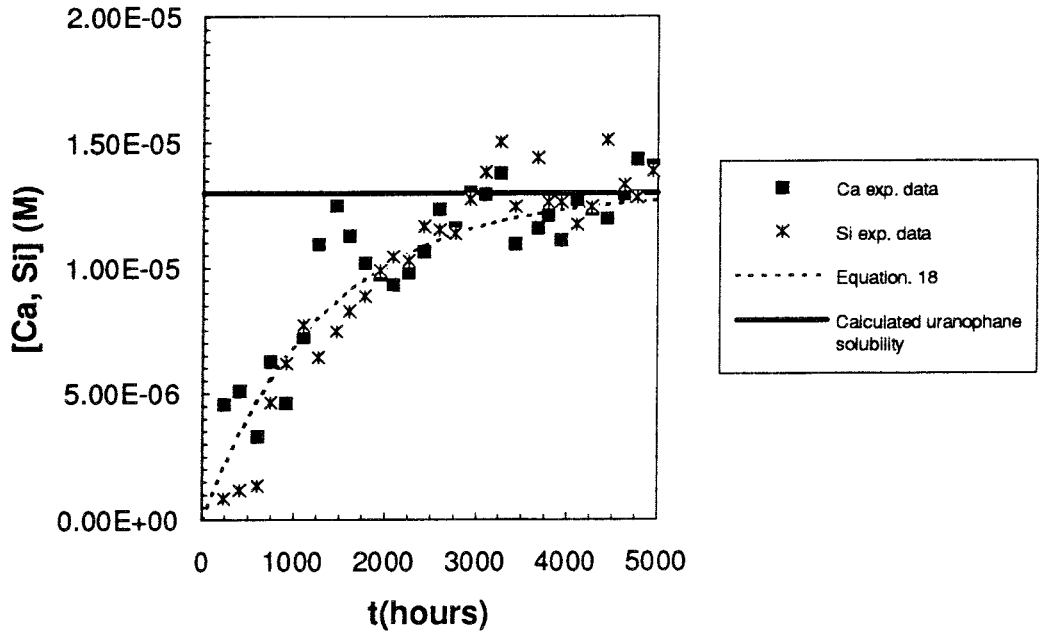

FIGURE 40

We examined this possible mechanism combining uranophane dissolution and soddyite precipitation.

This was done by using the geochemical code PHREEQE together with the HATCHES 5.0 database, in which the uranium database had been substituted by the SKBU. In addition, the logarithms of the solubility products of uranophane and soddyite were set to 7.78 and 3.01, respectively.

As input solution, we used pure water, but we fixed the pH at 7.3, which is approximately the average experimental pH for the first 5000 hours of the experiment. The calculations consisted on equilibrating the water to the two solid phases, in order to give the composition of a hypothetical solution in simultaneous equilibrium with uranophane and soddyite. The final solution composition calculated by the PHREEQE was:

$[Ca]_{tot} = 1.3 \cdot 10^{-5}$ mol dm^{-3}

$[Si]_{tot} = 1.3 \cdot 10^{-5}$ mol dm^{-3}

$[U]_{tot} = 1.25 \cdot 10^{-8}$ mol dm^{-3}

These solubilities are indicated in figures 39 and 40 by a solid line. These results clearly indicate the equilibrium proposed, and give confidence in the mechanism proposed for secondary phase formation, as well as to the solubility product constants presented. Certainly the final concentrations of Ca and Si are not exactly the same, because their stoichiometric ratio in uranophane is not the same, and Si, on the other hand, must precipitate together with uranium to form the new solid phase. However, the final result of the combination of the two processes leads to final concentrations for both elements that very similar, which corresponds to the experimental values.

The kinetics of the dissolution processes followed by the three elements to attain the corresponding equilibria have also been studied.

For Ca and Si, the rate of dissolution is assumed to follow a first-order rate equation. When equilibrium, or steady state, is achieved, this first order kinetics takes the form (Lasaga, 1981):

$$\frac{dC}{dt} = k \cdot (C_s - C) \qquad [16]$$

where C represents the concentration of the studied element for any time t, and C_s corresponds to the equilibrium or steady state concentration. The solution of the equation above, has the following expression:

$$\ln \frac{C_s - C}{C_s - C_0} = -k \cdot t \qquad [17]$$

where C_0 stands for the initial concentration of the element in solution. Assuming this initial concentration is equal to zero, since we worked in double distilled water, and rearranging equation [17], this has the final form:

$$C = C_s \cdot (1 - e^{-kt})$$

[18]

In this case, for Ca and Si, we used as C_s the value calculated by the PHREEQE code, and we determined the value of the rate constant that gave the best fit to the experimental values. By using a rate constant value of:

$$k = 7.5 \cdot 10^{-4}\ h^{-1}$$

we obtained the function presented in figure 40 as a dotted line.

For uranium we had to combine both a dissolution and a precipitation process. We used in both processes an expression similar to the one presented in equation [18], assuming for both reactions a first order kinetics. For the dissolution process, the value of C_s corresponded to the solubility limit of uranophane under the experimental conditions:

$$[U]_{eq}\ (\text{uranophane}) = 2.6 \cdot 10^{-5}\ \text{mol dm}^{-3}$$

with an initial concentration of zero.

For the precipitation process, we used a similar equation, but with a solubility limit of:

$$[U]_{eq}\ (\text{soddyite}) = 1.25 \cdot 10^{-8}\ \text{mol dm}^{-3}$$

In this case, the initial concentration was evidently not equal to zero, and we used as input the value calculated for the preceding dissolution process. By combining the two equations, we calculated the total uranium in solution as a function of time looking for the best fit to the experimental data (presented in figure 39 as a dashed curve). The values of the rate constants were:

$$k_{diss} = 6.5 \cdot 10^{-6}\ h^{-1}$$

$$k_{prec} = 8 \cdot 10^{-4}\ h^{-1}$$

On the other hand, the linear dashed line in figure 39 shows the trend that should be followed by uranium according to the initial dissolution rate, if there was no formation of a secondary phase.

From these data, the dissolution of Ca and Si occurs at faster rates than uranium. Although, as observed in figure 39, the best fits obtained for uranium follow the general trend of the experimental results but are not a good match to the measured values. Undoubtedly, the overall mechanism of combined reactions of dissolution-precipitation is quite complex, and we need more parameters to more closely represent the experimental data. However, we have shown that the general trend of the overall reaction is described by

the proposed mechanism of dissolution of the initial uranophane and the subsequent precipitation of soddyite after relatively short contact times.

Uraninite dissolution. Oxidizing conditions

The dissolution of the uraninite sample from Cigar Lake under oxidizing conditions is shown in figure 41 as total moles of uranium released in solution as a function of time.

The pH of the dissolution did not significantly change with the experimental time, giving values in the range of 7.9±0.2.

The dotted line in figure 41 shows the linear regression fit of the experimental data, which was constrained to pass through the origin, implying no uranium in solution at the beginning of the experiment. As observed, the representation follows a good linear behavior (when concentrations are plotted instead of moles), which implies a zeroth order kinetics of dissolution dependence during the experimental time. The expression of the rate of dissolution of zero order can be expressed in a simplified way as:

$$r_{diss} = \frac{d[U]}{dt} = k \qquad [19]$$

where **k** is the rate constant and includes any dependence, so far unknown, that the rate of dissolution may have on other experimental parameters (i.e., pH, complexing agents, redox potential, etc.). However, since the monitored conditions of the test solution were not observed to vary significantly during the experiment, we can combine these dependencies into a constant term. From equation 19, and considering as limits the uranium concentration equal to zero at time zero, we obtain:

$$[U] = k \cdot t \qquad [20]$$

which corresponds to a linear representation of the total uranium in solution versus time.

The solid phase characterization showed no evidence for compositional changes after the experiment, so we can assume that the determinations actually correspond to the dissolution of uraninite. According to the predominance diagrams shown in the previous section, under the experimental conditions we should see the formation of uranophane as a final

stable phase. Also, according to the previous solubility constant determined in this study, and using the calcium and silicon concentrations of the synthetic groundwater, we should reach a solubility of $7.6 \cdot 10^{-8}$ M (as calculated with PHREEQE). This value is clearly lower than the one actually reached in our experiment, which at the end of the experimental time was of $1.7 \cdot 10^{-5}$ M.

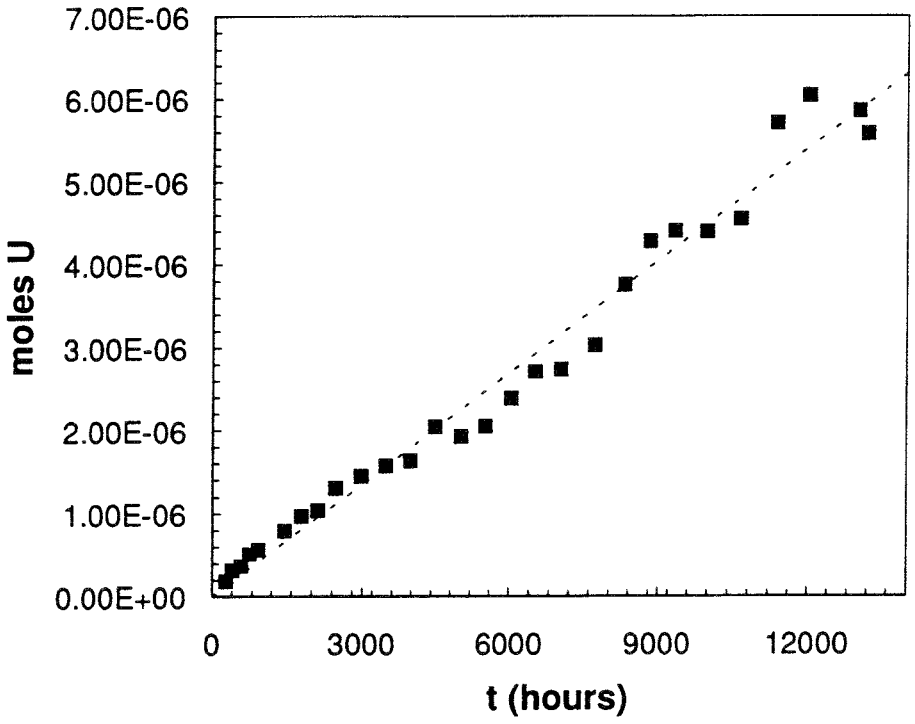

FIGURE 41

Thus, we must assume that the formation of uranophane is kinetically hindered, and that the formation of a secondary solid phase will go through the formation of a more favored phase. The secondary solid phase commonly found in the first instance is schoepite. The solubility limit of schoepite, calculated with the constant given above, is of $1.2 \cdot 10^{-3}$ M. This value is higher than the total uranium in solution at the end of the experiment. Accordingly, the formation of schoepite should not be observed, as it was clear from the sample characterization.

The linear regression shown in figure 41 has the following parameters:

slope: $4.5 \cdot 10^{-10}$ moles U h^{-1}

r^2: 0.978

The calculated slope is equivalent to the dissolution rate of uraninite under the experimental conditions. This value was normalized with respect of the

total surface area. To calculate this value, BET measurements were made to determine the specific surface area: $4.1(\pm0.2)\cdot10^{-2}$ m^2 g^{-1}. This measurement corresponds to the whole sample, that is, including the fractions not corresponding to uraninite (i.e., clay, galena,...). However, it is assumed to constitute a fair approximation of the uraninite surface area. This value was multiplied by the mass of solid used in the experiment (0.558g) to give the total area ($2.29\cdot10^{-2}$ m^2). Finally, the normalized rate of dissolution calculated was:

$$r_{diss} = 1.97\cdot10^{-8} \text{ moles U } h^{-1} m^{-2}$$

We compared this value with experiments performed in our laboratory with a chemical analogue of spent nuclear fuel (SIMFUEL) (Casas et al., 1991). However, the rates of dissolution given in that report must be corrected, since more recent determinations have proved that the actual specific surface area of the SIMFUEL pellets is much lower than the one given there. Hence, instead of the reported specific surface area of $1.5\cdot10^{-2}$ m^2 g^{-1}, a value of $1.92(\pm0.3)\cdot10^{-4}$ m^2 g^{-1} should be used. By applying this correction, the uranium rates of dissolution under oxidizing conditions for SIMFUEL are found to range between $4\cdot10^{-9}$ and $3\cdot10^{-8}$ moles U h^{-1} m^{-2}, values that are in a good agreement with the uranium rate of dissolution determined for the natural uraninite.

Uranophane dissolution. Oxidizing conditions

Total uranium in solution determined for uranophane as a function of time is presented in figure 42. The pH values during the experiment remained practically constant, within the range 7.9±0.1.

The dotted line in figure 42 gives the best linear regression of the experimental data. In this case the best fit could not be forced to pass through the origin. It is assumed that at the beginning of the experiment, we observed the rapid initial dissolution of more reactive phases. The parameters for this regression are:

slope:	$4.0\cdot10^{-11}$ moles U h^{-1}
y-intercept:	$1.11\cdot10^{-7}$ moles U
r^2:	0.958

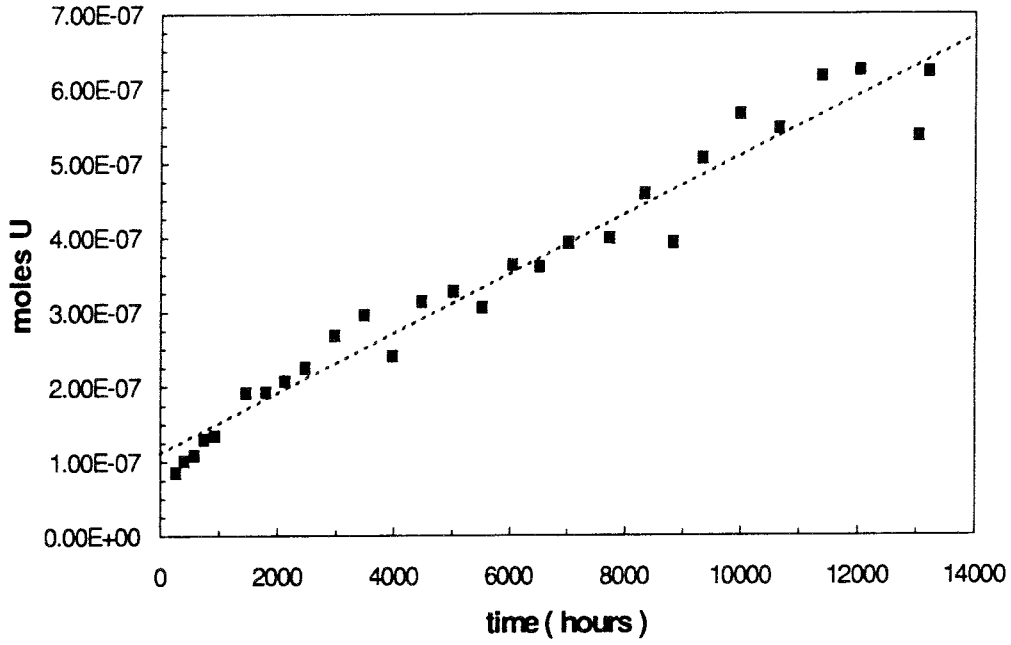

FIGURE 42

The representation of the uranium concentrations in the logarithmic form gave a poorer correlation than the one above. Therefore, considering that the regression parameter above indicates a good linear behavior of the data as a function of time, we conclude that the rate of dissolution can be considered as zero order with respect uranium and for the experimental time.

The specific surface area of this sample (notice here the same observations made for uraninite, related to the different fractions present in the solid phase) was also determined by the BET method, giving a value of: 0.29±0.02 $m^2\ g^{-1}$, which is one order of magnitude higher than that found for uraninite. From the mass of solid used in the experiment (0.0353 g), we calculate a total surface area of 0.01 m^2. Finally, the normalized dissolution rate calculated for uranophane is:

$$r_{diss} = 4.0 \cdot 10^{-9} \text{ moles U } h^{-1}\ m^{-2}$$

This value is only 5 times lower than that calculated for uraninite and is equivalent to the lowest rate of dissolution determined for SIMFUEL. These observations suggest that both phases have similar rates of dissolution, within the range of uncertainty of the determinations.

As determined in the previous section, the calculated solubility limit of this phase under the experimental conditions should be $7.6 \cdot 10^{-8}$ M, which is much lower than the uranium concentration determined at the end of the experiment:

$$[U] = 2.0 \cdot 10^{-6} \text{ M}.$$

The comparison of this experiment to the uranium in solution determined for the initial hours of dissolution of uranophane under anoxic conditions (shown also in figure 39), is shown in figure 43.

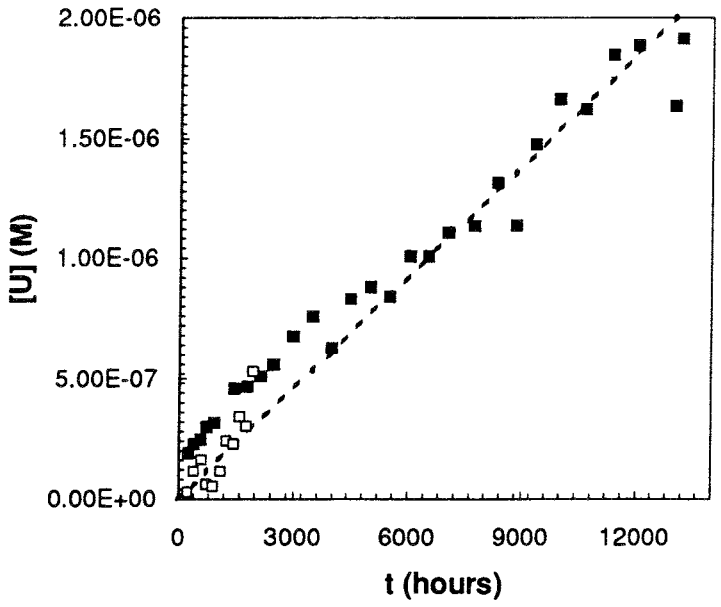

FIGURE 43

We can conclude that the initial rates of dissolution are quite similar in both cases, and the same linear model may fit fairly well both experiments. The main difference, however, is the subsequent behavior of uranium after the initial hours. Under anoxic conditions, we unambiguously observed the precipitation of a secondary solid phase identified as soddyite; under oxidizing conditions, secondary phase formation has not been observed, either by the solid phase characterization nor by the trend of the uranium released to solution. We still do not know whether the formation of the secondary phase was prevented by the presence of carbonate in the experiment under oxidizing conditions, that stabilized uranium in solution due to the formation of the highly stable uranium (VI)-carbonate complexes.

Schoepite dissolution. Oxidizing conditions

The experimental results obtained for the dissolution of this solid phase as a function of time are presented in figure 44.

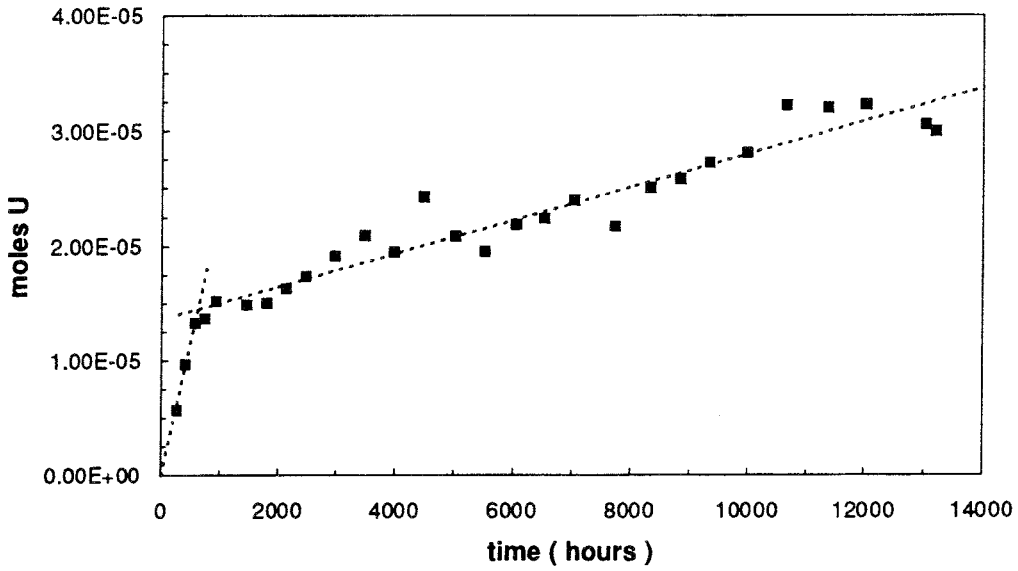

FIGURE 44

In this experiment, we also observed two different trends. At the beginning of the experiment we had a rapid initial dissolution rate, that we assume to be due to the initial presence of more reactive phases. After the initial 500 hours, approximately, the rate of dissolution decreased to a lower value that remained constant during the rest of the experiment. In both regions, the uranium release shows a nearly linear trend versus time, indicating, once again, the zero order of reaction with respect to uranium. The pH of the solution showed a slight though significant increase during the initial dissolution time. The average pH during the first 500 hours was 7.74±0.07, while for the rest of the experiment it was 8.00±0.10.

The initial linear adjustment was in this case successfully constrained to pass through the origin, and gave the following parameters:

slope: $2.3 \cdot 10^{-8}$ moles U h^{-1}

r^2: 0.992

After this initial dissolution, the linear parameters adjusted to the data were:

slope: $1.4 \cdot 10^{-9}$ moles U h^{-1}

y-intercept: $1.4 \cdot 10^{-5}$ moles U

r^2: 0.923

We observed approximately a one order of magnitude decrease between the first and the second rates of dissolution. Unfortunately, in this case we did not have enough sample to determine its specific surface area, so the values above cannot be normalized to compare them with the ones previously determined for uraninite and uranophane.

The uranium concentration determined at the end of the experiment was $9.2 \cdot 10^{-5}$ M, which is still lower than the solubility calculated for schoepite of $1.2 \cdot 10^{-3}$ M. If we recall at this point the characterization of the solid sample, it was found that a fine-grained white phase formed during the experiment, which resembled rutherfordine. The solubility of this solid phase, however, is even higher than the one corresponding to schoepite. According to the database used, the solubility limit of rutherfordine under the experimental conditions should be $4.7 \cdot 10^{-2}$ M.

As a pure modeling exercise we postulate a conceptual mechanism of the overall process as follows. We assume that three different main processes took place during the leaching period:

a.- A highly reactive phase initially present (i.e., fines) was rapidly dissolved during the first stage of the experiment. The limit of uranium dissolved is marked by the amount of this phase present at the beginning of the experiment, unless it exceeds the solubility limit of a more stable phase under the experimental conditions. This does not seem to be the case in our experiment, and we assume that it dissolved completely. The dissolution is assumed to follow equation 18, with C_s being no solubility limit, but the total amount of uranium present in the reactive phases.

b.- Once the first phase dissolved, schoepite began to dissolve approaching the solubility limit of $1.2 \cdot 10^{-3}$ M as calculated above. For this process, we assume a dissolution that follows first order kinetics, and again is governed by equation 18. However, because the solubility limit of schoepite is still much higher than the uranium content in solution during the experiment ($C_s >> C$ in eq. 18), a nearly linear model is obtained.

These two steps are considered to certainly match the dissolution of schoepite. Considering both of them together, we would obtain the dissolution process shown in figure 45 as a solid line.

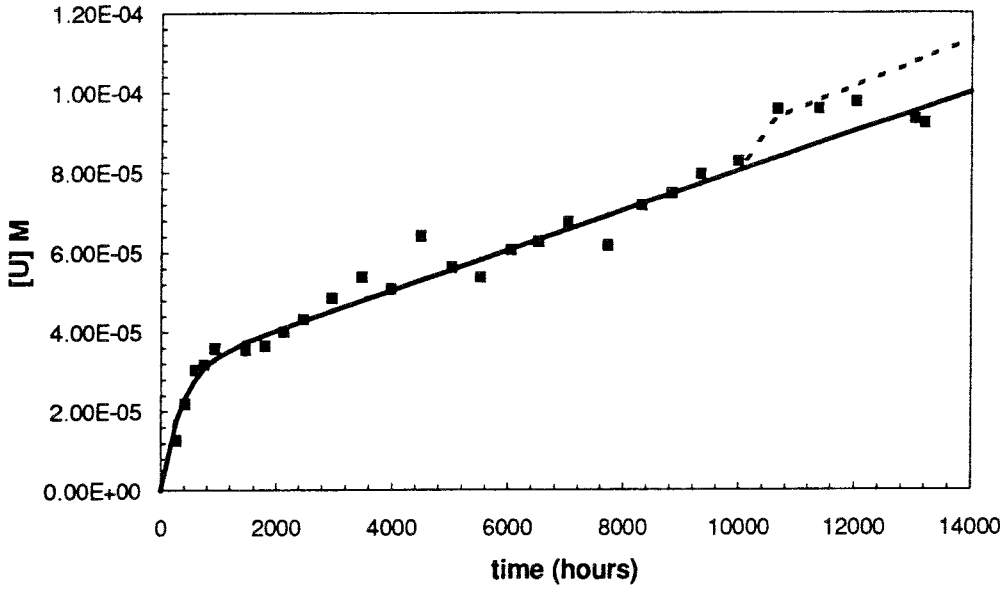

FIGURE 45

A third step is proposed trying to explain the solid phase observed on the schoepite surface after the leaching period.

c.- Due to the carbonate content, the solid phase starts to build up a secondary phase (i.e., rutherfordine), which increases the release of uranium in solution, being a more soluble phase. The presence of this solid phase may not be due to precipitation, because its solubility limit is much higher than the actual uranium determined in solution. Assuming rutherfordine appears at the last stage of the experiment, we calculated its dissolution as in the two preceding steps, using first order kinetics. The increase of uranium would follow the dotted line in figure 45.

The third step of the reaction mechanism is not definitely supported neither by the experimental data nor by the distinct identification of the precipitated solid phase, and it must be taken as purely speculative.

Some conclusions can be made by comparing the results obtained for the three samples studied under oxidizing conditions.

In general, the experiments carried out have shown that no significant changes in the solid phase composition took place during the experimental time (14000 hours). The only exception was for schoepite, where the formation of a secondary solid phase could be suspected. However, the uranium concentrations are in this case much higher than for the other two solids.

The dissolution rates for uraninite and uranophane are not significantly different, considering the structural and chemical differences between the two solids.

The formation of secondary solid phases was not observed, neither for uraninite nor for uranophane, though, from the thermodynamic point of view uranium in solution will lead to the formation of more stable solid phases, as it has experimentally been observed by earlier investigators (Wronkiewicz et al., 1992), and as it is indicated by the thermodynamic constants. The calculations show that uranophane is the more stable phase under the experimental conditions, and once it is formed, the uranium concentrations in solution will be given by the relatively low solubility of this phase. However, it is important to note that uranium can be released to a large extent before such phase is formed. This suggests that, in an oxidizing environment, thermodynamic constraints may take a long time before over coming kinetic release.

The value of the surface area to solution volume ratio (S/V) in the rate of formation of the possible secondary phases is of paramount importance. Macroscopically, a large surface will be in contact with small volumes of groundwater in a repository. Moreover, temperatures will also exceed the normal ambient temperature of our experiments. Determinations of Wronkiewicz et al. (1992), therefore, are valuable, since they have shown that the formation of secondary solid phases is relatively fast by using higher temperatures and small S/V ratios in their experiments. The formation of an initial schoepite led in their experiments to formation of more thermodynamically stable phases, such as silicates. This kinetic process is corroborated by our experiments.

CONCLUSIONS

The dissolution behavior of a series of uranium minerals has been studied. The samples were selected based on their potential usefulness in understanding the oxidative alteration of uraninite, as an analogy to the alteration pathway of the UO_2(s) in spent nuclear fuel.

The solid samples were extensively characterized by a wide variety of solid-state analytical techniques (SEM, TEM, XRD, EMPA, analytical optical microscopy). Bulk compositions, as well as surface characterizations, were performed for unleached samples and of solid phases after the experimental leaching period.

The solution analyses and solid phase characterizations have been integrated together and used to understand the mechanisms that controlled the leaching of the solid samples. However, it must be noted that the microscopic observations of the solids on an small scale (1-10 μm) are compared to a more macroscopic behavior measured in the solution of the leaching experiments.

The dissolution of uraninite under reducing conditions using a synthetic granitic groundwater, has shown the attainment of equilibrium over a range of pH values (4 to 9). By using selected uranium thermodynamic data, together with these experimental results, it is shown that there is a range of pH-pe values where reduced U(IV) is maintained in the solid phase while it may be oxidized to U(VI) in the aqueous phase, resulting in solubilities higher than expected for uraninite. This process is enhanced at neutral to alkaline pH values by the presence of carbonate in the leaching solution.

The dissolution of becquerelite under anoxic conditions in distilled water gives solubilities much lower than calculated by the solubility product constants found in the literature (Vochten and Van Haverbeke, 1990). A solubility product of 32.7±1.3 has been proposed based on the results of the dissolution experiments. This indicates that becquerelite should be thermodynamically more stable that schoepite, even at very low calcium concentrations. Calcium derived from becquerelite did not show a congruent dissolution behavior as compared with uranium, although, calcium was only analyzed in a few samples at acidic pH values.

The dissolution of three samples of uranophane under anoxic conditions using distilled water as a leachant showed different behaviors. The lowest solubility was obtained in a glass vessel. This is explained by silica leaching

from the glass walls. The other two experiments were completed in polyethylene bottles. One of them has allowed the calculation of a solubility product for uranophane of 7.8±0.8, which is consistent with values reported in the literature (Nguyen et al., 1992). However, the second experiment has shown a different behavior that has been explained by the formation of soddyite, also observed in the solid-state characterization after the leaching period. With the data obtained, a solubility product for soddyite of 3.0±2.9 has been suggested. The calcium, silicon and uranium concentrations determined in this experiment are consistent with a mechanism of dissolution of uranophane followed by the precipitation of soddyite, as was observed in the sample.

The kinetics of dissolution of uraninite, uranophane and schoepite have been determined under oxidizing conditions using a synthetic groundwater as a leaching solution. In general, the experiments carried out have shown that no significant changes in the solid phase composition occurred during the experimental time (14000 hours). The only exception was that of schoepite, in which the formation of a secondary solid phase (resembling rutherfordine, although not definitely identified) was suspected. The uranium concentrations were in this case much higher than for uraninite and uranophane.

The specific surface area of uraninite and uranophane samples has been determined by the BET method. Although, the measured values will include fractions not only corresponding to uranium minerals, they have been taken as a fair approximation to the actual value, and they have been used to calculate dissolution rates normalized with respect to the total surface area of the solid. This measurement could not be done on schoepite due to the lack of sufficient sample for a reliable BET measurement.

The dissolution rates determined for uraninite and uranophane are not very different, considering the structural and chemical differences between the two solids. The normalized dissolution rates obtained are:

$$r_{diss}(\textit{uraninite}) = 1.97 \cdot 10^{-8} \text{ moles } h^{-1} m^{-2}$$
$$r_{diss}(\text{uranophane}) = 4.0 \cdot 10^{-9} \text{ moles } h^{-1} m^{-2}$$

This suggests that the long term rate of dissolution under oxidizing conditions of the uranium phases does not depend critically on the composition of the solid phase. From the thermodynamic point of view, uranium in solution should lead to the formation of more stable solid phases, as has been

experimentally observed by previous investigators (Wronkiewicz et al., 1992), and as expected from the thermodynamic constants. The calculations show that uranophane is the most stable phase under the experimental conditions, and once it is formed, the uranium concentrations in solution will be controlled by the relatively low solubility of uranophane. However, uranium can be released to a large extent before such phases are formed. This suggests that, in an oxidizing environment, thermodynamic constraints may require a long time before overcoming the kinetic release.

The value of the surface area to solution volume ratio (S/V) in the rate of formation of the possible secondary phases is of paramount importance. A large solid surface will be in contact with small volumes of groundwater in a repository. Moreover, temperatures will also exceed the normal ambient temperature of our experiments. Determinations by Wronkiewicz et al. (1992), therefore, are valuable, as they have shown the relatively rapid formation of secondary solid phases, such as uranophane, by using higher temperatures and small S/V ratios in their experiments.

Future work should concentrate therefore in establishing the thermodynamics and kinetics of uranophane and soddyite synthetic samples to ascertain the final pathway for the long-term behavior of spent nuclear fuel under repository conditions.

Acknowledgements

This work has been finacially supported by SKB (Swedish Nuclear Fuel and Waste Management Co.) Solid state characterization (SEM, TEM, XRD, analytical EMPA) was completed in the Electron Microbeam Analysis Facility in the Department of Earth & Planetary Sciences at the University of New Mexico.

REFERENCES

Baes C.F. and Mesmer R.E. (1976); *The hydrolysis of cations*, John Wiley & Sons, Inc.

Bruno J. and Puigdomènech I. (1989); Mat. Res. Soc. Symp. Proc. **127**, 887-896

Bruno J., Casas I. and Sandino A. (1992); J. of Nuclear Mat. **190**, 61-69

Casas I., Sandino A., Caceci M.S., Bruno J. and Ollila K. (1991); *SIMFUEL dissolution studies in granitic groundwater* SKB Tech. Report **91-34**

de Pablo J., Duro L., Giménez J., Havel J., Torrero M.E. and Casas I. (1992); Analytica Chimica Acta **264**, 115-119

Finch R.J. and Ewing R.C. (1989); *Alteration of natural UO_2 under oxidizing conditions from Shinkolobwe, Katanga, Zaire: A natural analogue for the corrosion of spent fuel*, SKB Tech. Report **89-37**

Finch R.J. and Ewing R.C. (1991); *Uraninite alteration in an oxidizing environment and its relevance to the disposal of spent nuclear fuel*, SKB Tech. Report **91-15**

Finch R.J. and Ewing R.C. (1992); J. of Nucl. Mat. **190**, 133-156

Gayer K.H. and Leider H. (1957); Can. J. Chem. **35**, 5

Grenthe I., Fuger J., Lemire R., Muller A.B., Nguyen-Trung C. and Wanner H. (1990); *Chemical Thermodynamics of Uranium*, Nucl. Enrg. Agcy., Org. for Econ. Coop. and Dev.:Gif-sur-Yvette, France.

Janeczek J. (1991); N. Jb. Miner. Mh., **H. 9**, 385-395, Stuttgart 1991.

Janeczek J. and Ewing R.C. (1992); J. of Nucl. Mat. **190**, 157-173

Kraus K.A. and Nelson F. (1955); J. of Am. Chem. Soc. **77**, 3721

Langmuir D. (1978); Geochim. et Cosmochim. Acta **42**, 547

Lasaga A.C. (1981); *Kinetics of Geochemical Processes* (A.C. Lasaga and R.J. Kirkpatrick, eds.) Soc. Amer. Rev. Mineral, **8**, Washington D.C.

Lemire R.J. and Tremaine P.R. (1980); J. Chem. Eng. Data **25**, 361-370

Lemire R.J. (1988); AECL Report **AECL-9549**

Nguyen S.N., Silva R.J., Weed H.C. and Andrews J.E.,JR (1992); J. Chem. Thermodynamics **24**, 359-376

Robbins J.C. (1978a); Can. Inst. Mining and Metall. Bulletin **71**, 61-67

Robbins J.C. (1978b); Geo-Analysis'78

Sandino M.C.A. and Bruno J. (1992); Geochim. et Cosmochim. Acta **56**, 4135-4145

Vochten R. and Van Haverbeke L. (1990); Mineralogy and Petrology **43**, 65-72

Vochten R. (1991); Primary Radioactive Minerals, Theophrastus Publications S.A., Athens, Greece

Wronkiewicz D.J, Bates J.K., Gerding T.J., Veleckis E. and Tani B.S. (1992); J. of Nucl. Mat. **190**, 107-128

List of SKB reports

Annual Reports

1977-78
TR 121
KBS Technical Reports 1 – 120
Summaries
Stockholm, May 1979

1979
TR 79-28
The KBS Annual Report 1979
KBS Technical Reports 79-01 – 79-27
Summaries
Stockholm, March 1980

1980
TR 80-26
The KBS Annual Report 1980
KBS Technical Reports 80-01 – 80-25
Summaries
Stockholm, March 1981

1981
TR 81-17
The KBS Annual Report 1981
KBS Technical Reports 81-01 – 81-16
Summaries
Stockholm, April 1982

1982
TR 82-28
The KBS Annual Report 1982
KBS Technical Reports 82-01 – 82-27
Summaries
Stockholm, July 1983

1983
TR 83-77
The KBS Annual Report 1983
KBS Technical Reports 83-01 – 83-76
Summaries
Stockholm, June 1984

1984
TR 85-01
Annual Research and Development Report 1984
Including Summaries of Technical Reports Issued during 1984. (Technical Reports 84-01 – 84-19)
Stockholm, June 1985

1985
TR 85-20
Annual Research and Development Report 1985
Including Summaries of Technical Reports Issued during 1985. (Technical Reports 85-01 – 85-19)
Stockholm, May 1986

1986
TR 86-31
SKB Annual Report 1986
Including Summaries of Technical Reports Issued during 1986
Stockholm, May 1987

1987
TR 87-33
SKB Annual Report 1987
Including Summaries of Technical Reports Issued during 1987
Stockholm, May 1988

1988
TR 88-32
SKB Annual Report 1988
Including Summaries of Technical Reports Issued during 1988
Stockholm, May 1989

1989
TR 89-40
SKB Annual Report 1989
Including Summaries of Technical Reports Issued during 1989
Stockholm, May 1990

1990
TR 90-46
SKB Annual Report 1990
Including Summaries of Technical Reports Issued during 1990
Stockholm, May 1991

1991
TR 91-64
SKB Annual Report 1991
Including Summaries of Technical Reports Issued during 1991
Stockholm, April 1992

1992
TR 92-46
SKB Annual Report 1992
Including Summaries of Technical Reports Issued during 1992
Stockholm, May 1993

Technical Reports
List of SKB Technical Reports 1994

TR 94-01
Anaerobic oxidation of carbon steel in granitic groundwaters: A review of the relevant literature
N Platts, D J Blackwood, C C Naish
AEA Technology, UK
February 1994

TR 94-02
Time evolution of dissolved oxygen and redox conditions in a HLW repository
Paul Wersin, Kastriot Spahiu, Jordi Bruno
MBT Technología Ambiental, Cerdanyola, Spain
February 1994

TR 94-03
Reassessment of seismic reflection data from the Finnsjön study site and prospectives for future surveys
Calin Cosma[1], Christopher Juhlin[2], Olle Olsson[3]
[1] Vibrometric Oy, Helsinki, Finland
[2] Section for Solid Earth Physics, Department of Geophysics, Uppsala University, Sweden
[3] Conterra AB, Uppsala, Sweden
February 1994

TR 94-04
Final report of the AECL/SKB Cigar Lake Analog Study
Jan Cramer (ed.)[1], John Smellie (ed.)[2]
[1] AECL, Canada
[2] Conterra AB, Uppsala, Sweden
May 1994

TR 94-05
Tectonic regimes in the Baltic Shield during the last 1200 Ma - A review
Sven Åke Larsson[1,2], Eva-Lena Tullborg[2]
[1] Department of Geology, Chalmers University of Technology/Göteborg University
[2] Terralogica AB
November 1993

TR 94-06
First workshop on design and construction of deep repositories - Theme: Excavation through water-conducting major fracture zones Såstaholm Sweden, March 30-31 1993
Göran Bäckblom (ed.), Christer Svemar (ed.)
Swedish Nuclear Fuel & Waste Management Co, SKB
January 1994

TR 94-07
INTRAVAL Working Group 2 summary report on Phase 2 analysis of the Finnsjön test case
Peter Andersson (ed.)[1], Anders Winberg (ed.)[2]
[1] GEOSIGMA, Uppsala, Sweden
[2] Conterra, Göteborg, Sweden
January 1994

TR 94-08
The structure of conceptual models with application to the Äspö HRL Project
Olle Olsson[1], Göran Bäckblom[2], Gunnar Gustafson[3], Ingvar Rhén[4], Roy Stanfors[5], Peter Wikberg[2]
1 Conterra AB
2 SKB
3 CTH
4 VBB/VIAK
5 RS Consulting
May 1994

TR 94-09
Tectonic framework of the Hanö Bay area, southern Baltic Sea
Kjell O Wannäs, Tom Flodén
Institutionen för geologi och geokemi, Stockholms universitet
June 1994

TR 94-10
Project Caesium–An ion exchange model for the prediction of distribution coefficients of caesium in bentonite
Hans Wanner[1], Yngve Albinsson[2], Erich Wieland[1]
[1] MBT Umwelttechnik AG, Zürich, Switzerland
[2] Chalmers University of Technology, Gothenburg, Sweden
June 1994

TR 94-11
Äspö Hard Rock Laboratory Annual Report 1993
SKB
June 1994

TR 94-12
Research on corrosion aspects of the Advanced Cold Process Canister
D J Blackwood, A R Hoch, C C Naish, A Rance, S M Sharland
AEA Technology, Harwell Laboratory, Didcot, Oxfordshire, UK
January 1994

TR 94-13

Assessment study of the stresses induced by corrosion in the Advanced Cold Process Canister

A R Hoch, S M Sharland
Chemical Studies Department, Radwaste Disposal Division, AEA Decommissioning and Radwaste, Harwell Laboratory, UK
October 1993

TR 94-14

Performance of the SKB Copper/Steel Canister

Hans Widén[1], Patrik Sellin[2]
[1] Kemakta Konsult AB, Stockholm, Sweden
[2] Svensk Kärnbränslehantering AB, Stockholm, Sweden
September 1994

TR 94-15

Modelling of nitric acid production in the Advanced Cold Process Canister due to irradiation of moist air

J Henshaw
AEA Technology, Decommissioning & Waste Management/Reactor Services, Harwell, UK
January 1994